Mineralogy and Petrology (2007) 90: 109–140
DOI 10.1007/s00710-006-0166-0
Printed in The Netherlands

Mineralogy and Petrology

Contact metamorphism in the Los Santos W skarn (NW Spain)

S. M. Timón[1], **M. C. Moro**[1], **M. L. Cembranos**[1], **A. Fernández**[1], and **J. L. Crespo**[2]

[1] Departamento de Geología, Facultad de Ciencias, Universidad de Salamanca, Spain
[2] SIEMCALSA, Valladolid, Spain

Received August 10, 2004; accepted July 10, 2006
Published online September 12, 2006;
Editorial handling: R. Abart

Summary

The intrusion of the Lower Permian Los Santos-Valdelacasa granitoids in the Los Santos area caused contact metamorphism of Later Vendian-Lower Cambrian metasediments. High grade mineral assemblages are confined to a 7 km wide contact aureole. Contact metamorphism was accompanied by intense metasomatism and development of skarns, and it generated the following mineral assemblages: diopside, forsterite, phlogopite (±clintonite) and humites and spinel-bearing assemblages or diopside, grossular, vesuvianite ± wollastonite in the marbles, depending on the bulk rock composition. Cordierite, K-feldspar, andalusite and, locally, sillimanite appear in the metapelitic rocks. Mineral assemblages of marbles and hornfelses indicate pressure conditions ranging from 0.2 to 0.25 GPa and maximum temperatures between 630 and 640 °C. ^{13}C and ^{18}O depletions in calcite marbles are consistent with hydrothermal fluid–rock interaction during metamorphism. Calcites are depleted in both ^{18}O ($\delta^{18}O = 12.74‰$) and ^{13}C ($\delta^{13}C = -5.47‰$) relative to dolomite of unmetamorphosed dolostone ($\delta^{18}O = 20.79‰$ and $\delta^{13}C = -1.52‰$). The $\delta^{13}C$ variation can be interpreted in terms of Rayleigh distillation during continuous CO_2 fluid removal from the carbonates. The $\delta^{18}O$ values reflect hydrothermal exchange with an externally derived fluid. Microthermometric analyses of fluid inclusions from vesuvianite indicate that the fluid was water dominated with minor contents of CO_2 ($\pm CH_4 \pm N_2$) suggesting a metamorphic origin.

Fluorine-bearing minerals such as chondrodite, norbergite and F-rich phlogopite indicate that contact metamorphism was accompanied by fluorine metasomatism. Metasomatism was more intense in the inner-central portion of the contact aureole, where access to fluids was extensive. The irregular geometry of the contact with small aplitic intrusives between the metasediments and the Variscan granitoids probably served as pathways for fluid circulation.

Introduction

Emplacement of Variscan granitoid bodies of the Spanish Central System in Central Spain resulted in a contact metamorphic aureole in the host Later Vendian-Lower Cambrian metasediments and, in addition, lead to metasomatic activity related to the Los Santos skarn formation (Fig. 1). From cordierite + K-feldspar assemblages in hornfelses and gneisses, temperature and pressure conditions of the contact metamorphism were estimated between 600 and 640 °C and between 0.2 and 0.25 GPa (*Ugidos*, 1987). From wollastonite and sillimanite in calcsilicate rocks of the area and from the crystal chemical study of biotite and microcline of the granite, pressure conditions in the range of 0.15–0.38 GPa were derived for the time of granite emplacement. The temperature was estimated at 630–670 °C and X_{CO_2} between 0.25 and 0.5 (*Saavedra* and *García Sánchez*, 1973).

We present the textural, mineralogical and chemical characteristics of the mineral associations of the metamorphic rocks, which are located in the Los Santos contact aureole. We also ascertain the P–T–X_{CO_2} conditions at the deposit scale and establish its evolution during the associated metasomatism. Furthermore, we aim to determine the nature and the origin of the hydrothermal fluid and the degree of interaction with the host-rocks through the study of fluid inclusions and stable isotopes. Finally, we relate the contact aureole of the Los Santos skarn with others from the Spanish Central System (SCS) which are also accompanied by intense metasomatism and development of skarns.

Geologic setting

The study zone is located in Central Spain near the town of Salamanca. Geologically, the area pertains to the Spanish Central System (SCS), which is the most extensive continuous outcrop of granitoids in the Iberian Variscan Belt (Fig. 1a). It intruded into metasediments (dominantly schist and greywackes) of late Proterozoic-early Paleozoic age during the late- to post-main Hercynian tectonic events. At a regional level, the study area is located between metamorphic outcrops to the south of Salamanca and the northern part of the Bejar granites outcrop of the Central System. It consists mainly of a thick sequence of metamorphic sedimentary rocks and of igneous rocks (Fig. 1b). In this part of the Central System the igneous rocks are primarily granodiorites–monzogranites with minor granites. They define a calcalcaline series with an aluminous-cafemic tendency (*Rottura* et al., 1989), the genesis of which is discussed controversially. Some studies invoke mesocrustal anatectic processes (*Bea* and *Pereira*, 1990; *Pinarelli* and *Rottura*, 1995), while others suggest a mantle origin with metasediment assimilation (*Ugidos* and *Recio*, 1993).

In the Los Santos area, the country rock is mainly formed, from bottom to top, by a thick sequence of siliciclastic shales with frequent interbedded sandstones and conglomerates called the Complejo Esquisto Grauváquico (CEG) of Upper Proterozoic age (Monterrubio and Aldeatejada formations). This complex grades upwards into a Lower Cambrian, sandy and carbonate facies (Tamames Sandstone and Tamames Limestone formations). Overlying the carbonates, there is the Pizarras de Endrinal Formation. Stratigraphically, the highest position is represented by Ordovician and Silurian rocks, which outcrop in the cores of the Tamames and Endrinal Variscan synclines to the west and to the north of the study zone (*Díez*

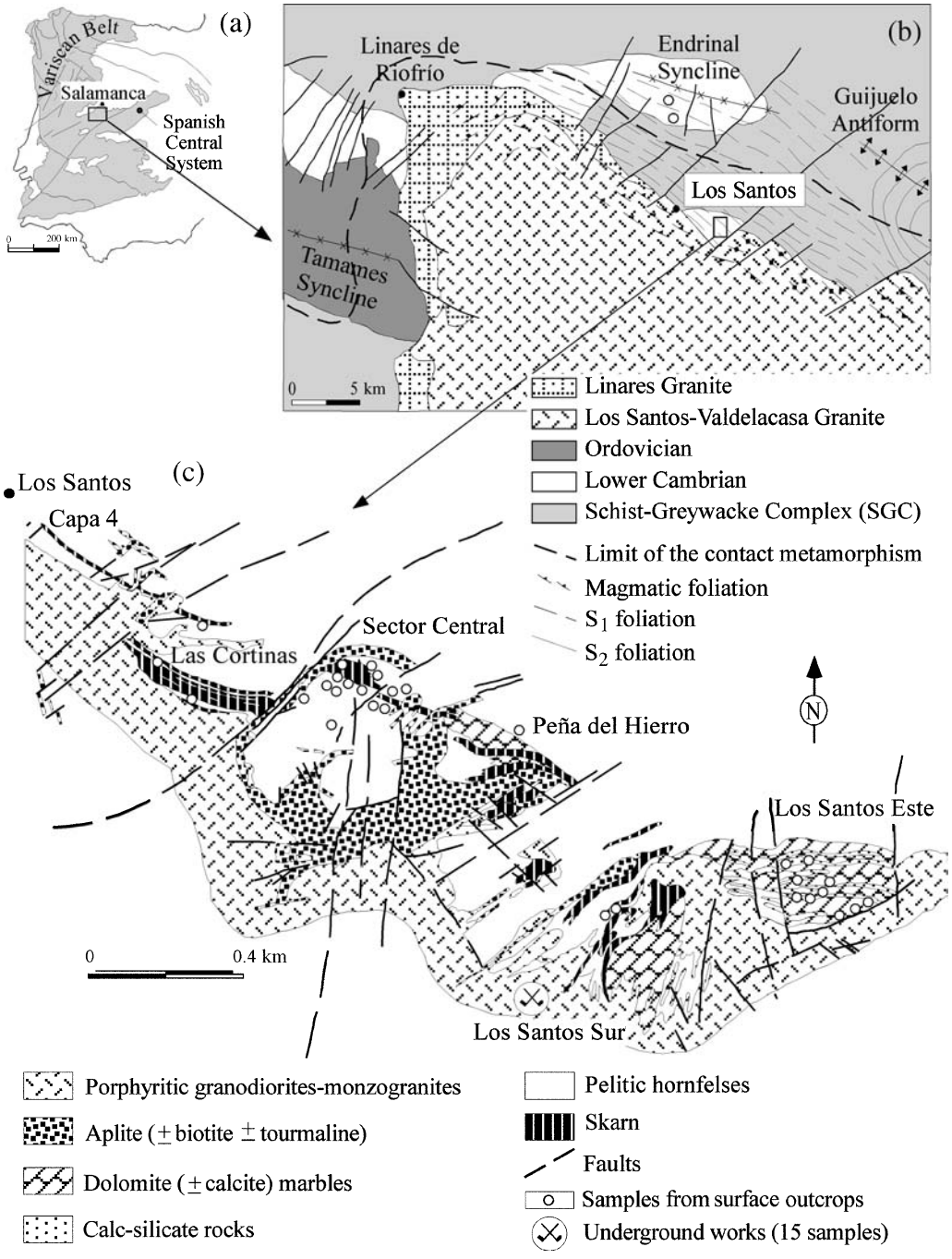

Fig. 1. (a) The Iberian Massif (*Julivert* et al., 1972) and location of the Spanish Central System (SCS). (b) Study area in the NW termination of the SCS with the limit of the contact metamorphic aureole and the magmatic foliation and the foliation outside of the thermal aureole (map from *Yenes* et al., 1996). (c) Geological sketch of the studied area with the location of the skarn and the samples studied

Balda, 1986). The igneous rocks of the study area consist of Los Santos porphyritic biotite granite, the Valdelacasa porphyritic biotite granite, which may contain cordierite and muscovite, and the Linares de Riofrio biotite granite (Fig. 1b). Sometimes they are crosscut by fine-grained porphyritic and biotite granites and tourmaline-bearing aplites and pegmatites (*Ugidos* and *Recio*, 1993). The contacts between the two porphyric facies are gradational while the contact of these with the Linares de Riofrio facies is sharper. No deformation has been observed at the contact between the different facies, indicating that the corresponding magmatic pulses and intrusion took place consecutively, but not too separated in time; i.e., before complete crystallization of the magma (*Yenes* et al., 1996).

The structural inventor of the country rocks can be explained by three superimposed Variscan deformation phases (*Díez Balda* et al., 1990): The first deformation phase (D_1) developed kilometre-scale folds with horizontal axes and vertical axial planes with an axial plane cleavage (S_1). The second phase (D_2) is related to extensional collapse of the previously thickened crust. This phase developed narrow shear zones, which outcrop in the area of Guijuelo (Fig. 1b). The age of this deformation phase is 332 ± 13 Ma (U–Pb in zircons) (*Galibert*, 1984). Lastly, the third deformation phase (D_3) was coaxial with D_1 but less pervasive, leading to large wavelength open folds with vertical axial planes and horizontal axes (S_3). The Guijuelo Antiform was formed during the D_3 deformation event (Fig. 1b).

Three episodes of regional metamorphism have been identified (*Díez Balda* et al., 1990): M_1 is an intermediate pressure Barrovian event, which is associated with crustal thickening during D_1, leading to the formation of chlorite, garnet, staurolite and sillimanite zone assemblages; M_2 is related to D_2 extension, it is a low pressure metamorphic event characterized by growth of andalusite and cordierite; lastly, M_3 is a retrograde event transforming biotite and chlorite to white mica indicating conditions close to the lower to mid greenschist facies, during D_3 compression. In addition to regional metamorphism, an aureole of contact metamorphism has developed, in the country rocks next to the granitic outcrops.

The ascent and emplacement of the Variscan granites took place after D_1 and D_2 because they cross-cut the structures developed during these phases. It probably occurred during the D_3 compressive stage, as suggested by the solid-state deformation observed in the granites and in the country rocks (*Yenes* et al., 1999). Rb–Sr and Sm–Nd analysis of the igneous rocks yielded ages of 300 Ma for the intrusions of the granitoids (*Pinarelli* and *Rottura*, 1995). Using K–Ar biotite analyses, *Yenes* et al. (1996) derived ages of 281 ± 6 and 280 ± 6 Ma for Linares granite and 269 ± 6 and 270 ± 6 Ma for the Los Santos-Valdelacasa granodiorites–monzogranites (referred to as Montemayor del Río pluton by the authors).

Contact metamorphic aureole and the Los Santos W-skarn

This aureole extends, in plain view (Fig. 1b), from 1.5 km to up to 8 km from the intrusive contacts. The aureole is defined by the occurrence of poikiloblastic cordierite crystals occasionally altered into pinnite in pelitic rocks. There is a first generation of cordierite that is ascribed to thermal effects of the Linares de Riofrío pluton. Subsequently, the intrusion of the Montemayor del Río pluton caused a horizontal crenulation and the simultaneous development of the second generation

of cordierite crystals. Other contact metamorphic minerals are biotite, muscovite and, locally, andalusite (*Yenes* et al., 1999). The variability of the width of the aureole in the vicinity of the Los Santos skarn could be related to the underlying granite and the associated thermal and fluid activity in the rocks around the skarn. In the Los Santos area the intrusive contact strikes NW–SE. It is subvertical and sub-parallel to the magmatic foliation (Fig. 1b). Gravity modelling of the pluton shape indicates an average thickness of 2 km for the Linares pluton and of 3 to more than 10 km for Los Santos-Valdelacasa (*Yenes* et al., 1999).

The W-bearing Los Santos skarn occurs, at the subvertical northern limb of the Tamames Syncline, along the contact between the Los Santos Valdelacasa granitoids and the Cambrian metasediments, and it is surrounded by the Aldeatejada Formation (SGC) (Fig. 1b). The deposit is intersected by a major NE–SW trending fault zone, which was active during granite emplacement and provided the necessary pathways for mineralizing fluids (Fig. 1c). Dominant igneous rocks are coarse-grained granodiorites and monzogranites. These rocks intruded as NE–SW trending dykes or as tens of metres-sized stocks, which correspond to fine grained biotite- and sometimes tourmaline-bearing granites. Within the deposit three Lower Cambrian lithologic units may be distinguished: the Areniscas de Tamames Formation, which grades upwards into the Calizas de Tamames Formation, and the Pizarras de Endrinal Formation. The rocks of the Calizas de Tamames Formation consist of an alternating sequence of dolomitic beds (30–50 cm thick) and minor limestone, which may grade laterally in to siliciclastic material, such as shales and greywackes. The only interstratified schists probably belong to the Pizarras de Endrinal Formation at Los Santos Sur (*Crespo* et al., 2000).

The skarn extends 3 km from the eastern end of the Los Santos town to the east. It displays a complex geometry due to faulting, and it was intruded by aplitic and microgranitic dykes. The most important fault is called Peña del Hierro, which divides the skarn deposit in two (Fig. 1c). To the east of this fault, carbonate beds form a periclinal closure dip 70–90° to the southeast, the two limbs of which are called Los Santos Sur and Los Santos Este. In the western part of the Peña del Hierro fault, known as Los Santos Oeste, the beds are subvertical and strike WNW–ESE. This section extends to the Los Santos village and is divided into three sectors by NE–SW striking faults. From west to east these sectors are known as Las Cortinas, Sector Central and Peña del Hierro (*Billiton Española*, 1985). We distinguish between exoskarn and endoskarn referring to sedimentary and igneous protolith, respectively. The exoskarn of the Los Santos deposit is irregular in shape and strata-bound in the metasediments. It is a hedenbergite exoskarn, which replaced dolomitic marbles, calcic marbles and hornfelses of the Cambrian sequence. The endoskarn is less pronounced. Where developed it is massive on the fine-grained biotite granite and consists of a quartz-feldspar alteration. Scheelite is frequently intergrown with the hedenbergitic clinopyroxene of the calcic exoskarn and it also appears in the retrograde skarn superimposed onto the earlier.

Samples and methods

Sampling for this study was focussed underground. The surface geology was studied previously by *Billiton Española* (1985) for the economic evaluation of the

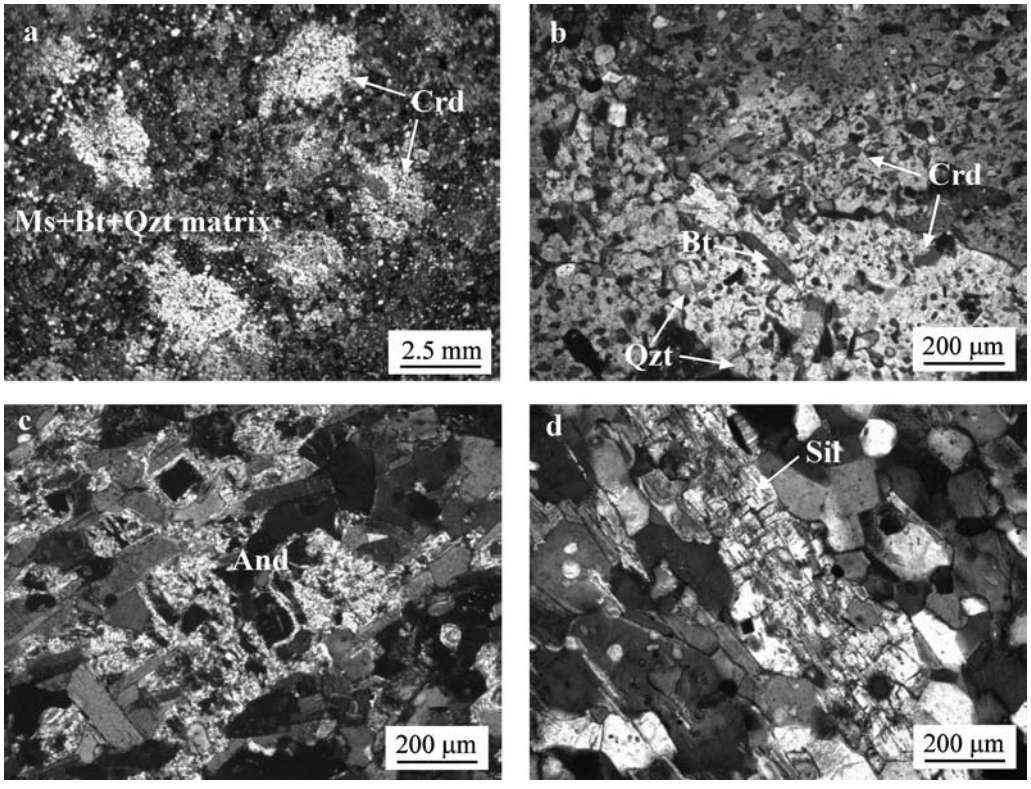

Fig. 2. Photomicrographs of the mineral assemblages in the hornfelses. (a) Porphyroblasts of cordierite (Crd) in a fine-grained matrix; (b) poikiloblastic cordierite grains with numerous inclusions of quartz and biotite; (c) andalusite (And) altered to sericite; (d) sillimanite (Sil) prismatic crystal transformed into sericite

deposit. The forty samples of marbles and hornfelses from surface outcrops are indicated in the geological sketch map of the Los Santos skarn (Fig. 1c). In Table 1 the location, the lithology and the mineral assemblages are summarised for all the samples studied. More than 50 polished thin sections were prepared to study the textural, mineralogical and chemical variations across the metamorphic zone. 9 representative samples of marbles were selected for separation of calcite for stable isotope analysis and 3 representative samples of dolomite from outside the contact aureole were selected for stable isotope analyses of unaltered dolomite. Lastly, 2 representative samples of calcic marble were selected for study of fluid inclusions in vesuvianite.

The mineral contents and textural relationships between the different metamorphic rocks were determined using optical polarization microscopy, powder XRD, scanning, as well as transmission electron microscopy (SEM and TEM) coupled to an energy dispersive X-ray analysis system (EDX). Moreover, quantitative mineral analysis was carried out on carbon-coated thin section using a JEOL JM-6400 electron microprobe run at an acceleration voltage of 15 kV and 10 nA beam current with a beam diameter of 5 µm. Calibration was done using pure metals and mineral as well as synthetic standards. These tasks were carried out at the University of Salamanca and Madrid (Servicios Generales de Microscopía

Electrónica). Chemical formulae of all minerals and the end-member proportions for clinopyroxene, olivine and garnet were calculated from mineral analyses according to the method of *Deer* et al. (1992). Total iron is reported as total FeO and Fe^{3+} is estimated based on stoichiometry.

Fluid inclusions were studied on wafers (300 μm thick) of vesuvianite from representative samples of the calcite marbles by petrographic and microthermometric means. For microthermometry a Chaixmeca heating-freezing stage was used. The stage was calibrated using known melting points of solid standards at $T > 25\,^{\circ}C$ on natural and synthetic fluid inclusion at $T < 0\,^{\circ}C$. The rate of heating was monitored to obtain an accuracy of $\pm 2\,^{\circ}C$ during freezing, and $\pm 4\,^{\circ}C$ upto $400\,^{\circ}C$.

The carbon and oxygen isotope compositions of selected samples were determined at the laboratories of the Servicio General de Análisis de Isótopos Estables, University of Salamanca. These samples were subjected to hand-picking under a binocular microscope. The powder X-ray diffraction (XRD) method was used for checking the purity of minerals. Extraction of CO_2 from carbonates for isotopic analysis followed standard techniques (*McCrea*, 1950; *Craig*, 1957) and was achieved by reacting about 10 mg of carbonate with 100% H_3PO_4. Isotopic ratios were measured in a VG-Isotech SIRA-II mass spectrometer. The average precision obtained was $\pm 0.2‰$ (1σ) ($\delta^{13}C$ and $\delta^{18}O$). Oxygen and carbon isotope compositions are reported in standard per mil notation relative to V-SMOW (Vienna Standard mean ocean water) and V-PDB (Vienna Peedee belemnite), respectively.

Contact metamorphism and metasomatism

The hornfelses

The hornfelses originated during contact metamorphism from pelitic rocks previously metamorphosed under regional metamorphism conditions to the greenschist facies. The protolith mineralogy of the hornfelses consists of biotite, chlorite, muscovite, quartz, plagioclase, tourmaline, zircon, ilmenite and carbonaceous matter. Given that these metapelite layers alternate with other more psammitic layers, cordierite-rich and quartzfeldspatic layers are developed during contact metamorphism, respectively.

Contact metamorphism of the pelitic layers has resulted in the appearance of cordierite, K-feldspar, andalusite and locally sillimanite. The most important phases in hornfelses are summarized in Table 1.

Cordierite–K-feldspar–andalusite ± sillimanite hornfelses. Macroscopically, these hornfelses are dark grey in colour, compact and fine-grained. Sometimes they show a light banding but frequently they exhibit the typical spotted texture, in other words, equally distributed millimetre sized nodules and a banding defined by aligned micas can be observed. Sillimanite-bearing hornfelses only appear in the Peña del Hierro sector. Microscopically these rocks consist of quartz, biotite, moscovite, K-feldspar, plagioclase and cordierite, which occur in a fine-grained granoblastic matrix. Poikilitic cordierite and andalusite porphyroblasts have numerous inclusions of quartz and biotite (Fig. 2a, b). Biotite, is very abundant and displays a lepidoblastic texture by mimetic growth reproducing a pre-metamorphic struc-

Table 1. *Location, lithology, sample number and summary of the mineral assemblages in marbles and hornfelses from Los Santos. The different study areas can be identified from Fig. 1b, c*

Area	Lithology type	Samples location	Sample number	Cal	Dol	Cpx	Fo	Chn	Nrb	Ves	Grt	Wo	Phl	Prg	Clin	Qtz	Kfs	And	Pl	Ms	Bt	Crd	Sil	Spl	Mgt	Chl
Endrinal Syncline	Metapelite	Outside of the contact metamorphic aureole	925 (2)													x			x	x	x					x
	Low grade metamorphic dolomite		926 (3)		x								x			x				x						x
	Low grade metamorphic limestone		927 (3)	x												x			x	x						x
Los Santos Este	Fo-Di-Phl marbles	Samples from surface outcrops taken inside the contact metamorphic aureole, next to the intrusive contact (0–30 m)	958 (2)	x		x							x	x	x										
			959 (2)	x	x	x	x						x											x		
	Di-Grs-Vsv ± Wo marbles		960, 1696, 1697, 1698, 1702, 1703	x		x				x	x	x	x													
	Hu-Spl-Fo marbles		908, 909, 917, 918, 920	x	x		x	x	x				x											x	x	x
Sector Central	Di-Grs-Vsv ± Wo marbles		917B, 1652, 1653	x		x				x	x	x	x													
Peña Del Hierro	Crd-Kfs-And ± Sil hornfelses		943, 901, 903, 924, 925, 1379													x	x	x			x	x				
La Capa 4			954													x					x	x	x			
Las Cortinas Oeste			964													x	x	x			x	x				
			930													x	x				x	x				
Los Santos Sur	Hu-Spl-Fo marbles	Underground samples taken inside the contact metamorphic aureole, next to the intrusive contact	971, 974, 975, 1649, 1651, 1654, 1686, 1693, 1694													x	x	x			x	x				
			972, 973, 977	x	x		x	x	x				x													x
	Di-Grs-Vsv ± Wo marbles		2733,1647, 1648	x		x				x	x	x														

Mineral abbreviations are after *Kretz* (1983); *x* present phase

Table 2. *Selected microprobe analyses (in wt.%) of cordierite (Crd), biotite (Bt), white mica (Ms) and feldspar (Kfs) from the hornfelses; cations for Crd are calculated on the basis of 18 oxygens, for Kfs on the basis of 8 oxygens and for micas on the basis of 22 oxygen atoms*

Mineral	Crd	Bt	Kfs	Ms
Sample	925	925	925	1379
Spot	2.50	P48	1.46	2.5
SiO_2	47.39	35.35	64.36	47.92
TiO_2	0.03	3.37	0.02	0.00
Al_2O_3	32.61	19.75	18.59	33.90
FeO*	7.19	15.94	0.05	1.13
MnO	0.11	0.03	0.03	0.04
MgO	7.17	8.36	0.00	0.27
CaO	0.04	0.06	0.06	0.04
BaO	0.00	–	0.57	0.00
SrO	0.30	0.20	0.37	–
Na_2O	1.22	0.10	1.38	0.14
K_2O	0.15	9.24	14.09	10.68
F	0.00	0.51	–	0.00
Total	96.20	92.91	99.52	94.11
Si	4.96	5.39	2.98	6.42
Ti	0.00	0.39	0.00	0.00
Al	4.02	3.55	1.02	2.92
Fe^{2+}	0.59	2.03	0.00	5.36
Mn	0.01	0.00	0.00	0.00
Mg	1.12	1.90	0.00	0.05
Ca	0.00	0.01	0.00	0.01
Ba	0.00	–	0.01	0.00
Sr	0.02	0.00	0.01	–
Na	0.25	0.03	0.12	0.04
K	0.00	1.80	0.83	1.83
Total	10.97	15.10	4.97	13.83
F	0.00	0.25	–	0.00

* Total Fe = Fe^{2+}

ture. Sillimanite appears as prismatic crystals. Andalusite and sillimanite are commonly transformed to sericite (Fig. 2c, d). In Table 2 the cordierite and biotite chemical compositions are summarized. In cordierite, X_{Mg} is between 0.69 and 0.81 while in biotite X_{Mg} is 0.48. Feldspar ($Or_{0.85}$) has a $K/(K+Na)$ ratio of 0.87. Selected microprobe point analyses of feldspar and muscovite are given in Table 2. Tourmaline, rutile, ilmenite, apatite, zircon, titanite, pyrrhothite, chalcopyrite, pyrite and magnetite are present as accessory minerals. Secondary minerals are sericite, muscovite and chlorite. Feldspar, plagioclase and andalusite are altered to sericite, biotite is altered to chlorite and cordierite shows the typical alteration to pinnite, and sometimes it is transformed into an aggregate of magnesian chlorite and white mica.

The dolomite marbles

The protolith of these metamorphic rocks has been studied in samples from the Endrinal syncline (outside the metamorphic aureole, Fig. 1b). It corresponds to siliceous dolomite beds, which are only affected by low-grade regional metamorphism and retain original sedimentary and diagenetic textures. They consist of dolosparites with alternations of siliceous beds. Dolosparites contain 73–98% dolomite, 0.8–13% quartz, 1–13% phyllosilicates (phlogopite, muscovite and chlorite), with minor (<1%) plagioclase, calcite, tourmaline, zircon and pyrite. The dolomite is Fe-rich. Its medium grain size is 110 μm, and it shows a granoblastic, nearly equigranular texture. Generally, quartz and phyllosilicates occur as accessory minerals but they may form fine layers without lateral continuity.

The predominant mineral assemblage developed during contact metamorphism of this dolomitic protolith is calcite–dolomite–diopside–forsterite–phlogopite. Less common, more silica-rich dolomitic marbles contain the assemblage pargasite–calcite–diopside–phlogopite. This latter assemblage, which only appears at Los Santos Este, contains clintonite and chlorite. Locally, forsterite-norbergite and/or chondrodite-spinel paragenesis occurs. Diopside is absent from this association. Phlogopite is nearly ubiquitous in all samples of the dolomitic marbles. Magnetite, fluorapatite, pyrrhotite, chalcopyrite, and arsenopyrite are present as accessory minerals. Magnesian chlorite, serpentine, epidote-group minerals occur as alteration minerals. The most important dolomitic marble mineral phases are summarized in Table 1.

Forsterite–diopside–phlogopite marbles occur in the Los Santos Este zone. Banding and recrystallization are observable in hand specimen. Some bands are of a white-greyish colour coarse-grained carbonate rich, and others are fine-grained and have a beige colour corresponding to more siliceous bands (Fig. 3a). Sometimes the original sedimentary layering is obscured by recrystallization. The carbonate matrix is characterized by a fine-grained mosaic of carbonate grains and smaller forsterite, diopside and phlogopite grains at triple junctions of carbonate grains (Fig 3c). These marbles are characterized by the appearance of forsterite-rich olivine, typical for metamorphosed impure dolomites (Table 3). Forsterite occurs as equigranular and rounded 5–10 μm grains. The diopside occurs as anhedral to subhedral crystals. The chemical composition of diopside ($Di_{0.91-0.94}$) is summarized in Table 3. Phlogopite occurs as layered aggregates of platy crystals with dark-green colours. In general, phlogopite shows straight extinction under crossed polarizers and, sometimes, it is altered to secondary chlorite. The chemical composition of phlogopite is shown in Table 3 (sample 959). In this assemblage, it doesn't show any fluorine and $Mg/(Mg + Fe) = 0.96$. There are amphibole crystals, which correspond to tremolite according to the classification of *Leake* et al. (2004) (Table 4). In these forsterite-diopside-phlogopite marbles sulphides are present at < 1 vol.% mainly pyrrothite and chalcopyrite.

In addition to these characteristic minerals clintonite and pargasite may be present (Fig. 3b). Clintonite occurs as elongate crystals, it is nearly colourless in plane-polarized light, showing straight extinction under crossed polarizers. Clintonite is Mg-rich, containing small amounts of Fe ($X_{Mg} = 0.94$) and has an X_F ranging from 0.03 to 0.09 (Table 3). The clintonite compositions lie close to the

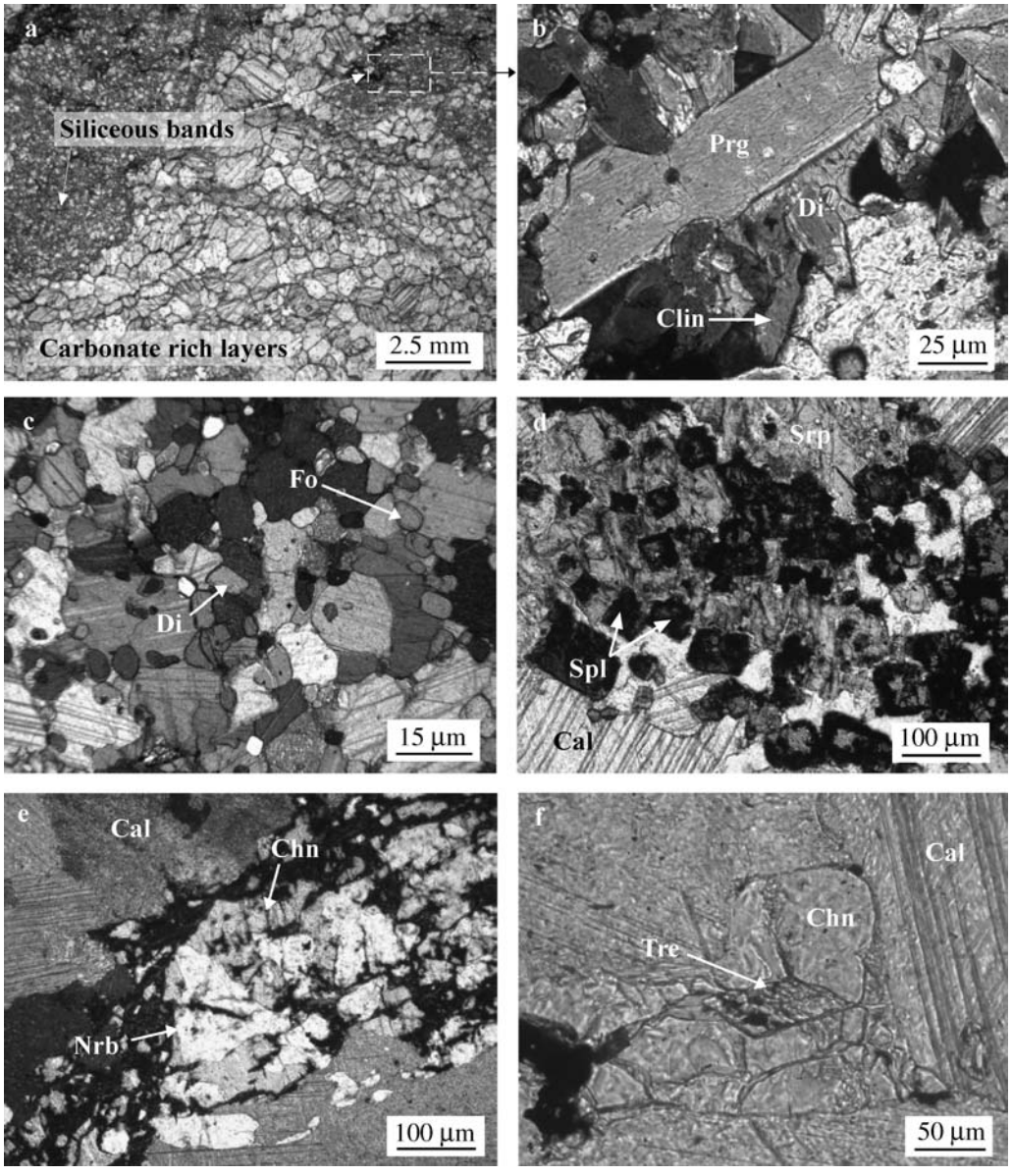

Fig. 3. (a) Portion of a dolomite marble from Los Santos Este; coarse-grained layers are recrystallized carbonates and the fine-grained ones are an aggregate of carbonates, diopside (Di), phlogopite (Phl), clintonite (Clin) and pargasite (Prg) (Photo b). Photomicrographs (b, c, d, e and f) in transmitted light illustrating textural relationships in dolomite marbles; (c) forsterite and diopside grains associated with carbonates in forsterite–diopside–phlogopite marbles; (d) serpentinized forsterite (Srp) and spinel (Spl) in a carbonate matrix; (e) chondrodite (Chn) and norbergite (Nrb) intergrowth; (f) basal section of tremolite (Tre) associated with chondrodite and calcite (Cal); (d), (e) and (f) humite-, spinel-bearing assemblages in forsterite–phlopite marbles. (a), (d) and (f) under parallel polarizers; (b), (c) and (e) under crossed polarizers

Table 3. *Microprobe analyses of forsterite, clinopyroxene, phlogopite and clintonite from the dolomite marbles; forsterite formula based on 4 oxygens, clinopyroxene formula based on the basis of 6 oxygens, phlogopite and clintonite formulae based on 22 oxygen atoms*

Mineral	Forsterite			Clinopyroxene			Phlogopite			Clintonite		
Sample	959	959		958	958	958	908	908	959	958	958	958
Spot	1.41	1.55		2.63	2.64	3.65	1.3	3.9	2.47	3.70	3.71	3.72
SiO_2	40.83	41.13		50.12	53.95	53.01	39.50	40.06	38.91	18.36	18.82	18.25
TiO_2	0.00	0.00		0.55	0.02	0.30	0.07	0.16	0.30	0.19	0.28	0.30
Al_2O_3	0.03	0.00		4.99	0.22	1.83	14.33	13.88	17.27	40.68	40.14	41.01
FeO*	7.27	6.95		2.57	2.16	1.59	5.02	3.55	1.88	2.25	2.30	2.21
MnO	0.09	0.09		0.05	0.00	0.01	0.03	0.06	0.01	0.02	0.02	0.00
MgO	49.91	50.39		15.11	16.81	16.55	25.31	25.66	23.96	19.57	19.79	19.23
CaO	0.07	0.06		26.59	26.42	26.53	0.08	0.11	0.05	12.77	12.78	12.96
Na_2O	0.00	0.01		0.05	0.05	0.00	0.48	0.18	0.67	0.29	0.30	0.29
K_2O	0.00	0.02		0.00	0.02	0.00	9.28	10.02	9.88	0.01	0.02	0.04
F	–	–		–	–	–	1.93	1.49	0.00	0.24	0.15	0.40
Cl	–	–		–	–	–	0.02	0.02	0.02	0.01	0.00	0.01
Total	98.19	98.66		100.0	99.65	99.81	96.04	95.19	92.95	94.38	94.61	94.70
Si	1.01	1.01		1.84	1.98	1.94	5.46	5.59	5.59	2.61	2.67	2.58
Ti	0.00	0.00		0.02	0.00	0.01	0.01	0.02	0.03	0.02	0.03	0.03
Al	0.00	0.00		0.22	0.01	0.08	2.34	2.28	2.92	6.81	6.71	6.84
Fe^{2+}	0.15	0.14		0.08	0.07	0.05	0.58	0.41	0.23	0.27	0.27	0.26
Mn	0.00	0.00		0.00	0.00	0.00	0.00	0.01	0.00	0.00	0.00	0.00
Mg	1.83	1.84		0.83	0.92	0.90	5.22	5.34	5.13	4.14	4.19	4.06
Ca	0.00	0.00		1.05	1.04	1.04	0.01	0.02	0.01	1.94	1.94	1.96
Na	0.00	0.00		0.00	0.00	0.00	0.13	0.05	0.19	0.08	0.08	0.08
K	0.00	0.00		0.00	0.00	0.00	1.64	1.78	1.81	0.00	0.00	0.01
Total	2.99	2.99		4.03	4.02	4.01	15.38	15.49	15.90	15.88	15.90	15.82
F	–	–		–	–	–	0.84	0.66	0.00	0.11	0.07	0.18
Cl	–	–		–	–	–	0.01	0.01	0.00	0.00	0.00	0.00
OH	–	–		–	–	–	1.15	1.34	2.00	1.89	1.93	1.82
X_{Mg}	0.92	0.93		0.91	0.93	0.95	0.90	0.93	0.96	0.94	0.94	0.94
X_F	–	–		–	–	–	0.42	0.33	0.00	0.05	0.03	0.09
Fo	92.4	92.8	Di	91.1	93.3	94.9						
Fa	7.6	7.2	Hd	8.7	6.7	5.1						
			Jh	0.0	0.0	0.0						

* Total Fe = Fe^{2+}

MgSi-rich end-member of the solid solution series synthesized by *Olesh* (1975) and they are Al-poor. The textural relationships observed indicate that clintonite was formed in equilibrium with forsterite, diopside and phlogopite. In these layers, small amounts of hornblende occur as idiomorphic crystals <25μm in length (Fig. 3b). These hornblende crystals exhibit a distinct pleochroism in greenish colours. According to the classification of *Leake* et al. (2004) this hornblende corresponds to pargasite. It has an X_{Mg} between 0.84 and 0.89 and a X_F between 0.02 and 0.06 (Table 4).

Table 4. *Microprobe analyses of chlorite and amphiboles from dolomite marbles; amphibole structural formulae is estimated following the procedure of* Robinson *et al. (1982) on the basis of 13 cations; Fe^{3+} is calculated by charge balance. Chlorite analyses normalized to 18 (O, OH, F, Cl) and Fe^{3+} is calculated according to* Hendry *(1981)*

Mineral	Chlorite				Pargasite				Tremolite	
Sample	909	909	909	920	958	958	958	958	959	959
Spot	2.6	2.8	5.20	4.29	2.61	3.66	3.67	3.68	1.3	2.5
SiO_2	28.71	27.66	33.49	28.90	40.14	40.74	41.06	41.35	56.60	55.60
TiO_2	0.12	0.08	0.00	0.00	0.54	0.77	0.93	0.77	0.13	0.06
Al_2O_3	21.13	24.55	13.21	21.19	18.57	16.77	16.90	15.39	3.34	5.43
FeO	11.00	14.15	7.31	6.52	5.29	3.80	4.22	4.54	0.53	0.48
MnO	0.18	0.25	0.04	0.07	0.01	0.00	0.03	0.03	0.00	0.00
MgO	26.22	19.60	32.24	29.82	15.06	16.65	16.63	16.88	23.40	23.10
CaO	0.06	0.18	0.30	0.03	13.70	13.66	13.57	13.82	13.20	13.20
Na_2O	0.04	0.41	0.02	0.02	2.24	2.45	2.38	2.55	0.20	0.19
K_2O	0.03	0.04	0.07	0.01	1.24	1.30	1.23	0.73	0.14	0.10
F	0.68	0.10	0.62	0.77	0.26	0.24	0.19	0.08	0.56	0.60
Cl	0.02	0.01	0.03	0.02	0.06	0.04	0.08	0.05	–	–
Total	88.07	87.37	87.30	87.17	97.39	96.74	97.54	96.47	98.10	98.76
Si^{IV}	3.13	2.79	3.58	3.16	5.84	5.94	5.93	6.04	7.69	7.52
Al^{IV}	0.87	1.21	0.42	0.84	2.16	2.06	2.07	1.96	0.31	0.48
Ti	0.01	0.01	0.00	0.00	0.06	0.08	0.10	0.08	0.01	0.01
Al^{VI}	1.84	1.71	1.24	1.89	1.03	0.82	0.81	0.68	0.23	0.39
Fe^{3+}	0.00	0.00	0.00	0.00	0.00	0.00	0.00	0.00	0.00	0.00
Fe^{2+}	1.00	1.19	0.65	0.60	0.64	0.46	0.51	0.55	0.06	0.05
Mn	0.02	0.02	0.00	0.01	0.00	0.00	0.00	0.00	0.00	0.00
Mg	4.26	2.95	5.13	4.86	3.27	3.62	3.58	3.67	4.74	4.65
Ca	0.01	0.02	0.03	0.00	0.14	0.14	0.10	0.16	1.93	1.91
Na	0.01	0.08	0.00	0.00	0.63	0.62	0.67	0.70	0.02	0.02
K	0.00	0.01	0.01	0.00	0.23	0.24	0.23	0.14	0.06	0.05
Total	11.15	9.99	11.07	11.36	13.00	12.99	13.00	12.99	13.04	13.10
F	0.23	0.03	0.21	0.27	0.12	0.11	0.08	0.04	0.24	0.26
Cl	0.00	0.00	0.01	0.00	0.02	0.01	0.02	0.01	–	–
OH	7.76	7.97	7.79	7.73	1.86	1.88	1.90	1.95	1.76	1.74
X_{Mg}	0.81	0.71	0.89	0.89	0.84	0.89	0.88	0.87	0.99	0.99
X_F	0.029	0.004	0.026	0.033	0.06	0.06	0.04	0.02	0.12	0.13

Locally humite- and spinel-bearing assemblages also appear in forsterite marbles. In the hand sample they are whitish coarse-grained rocks with other more fine-grained layers. Millimetre sized idiomorphic magnetite crystals and honey coloured forsterite crystals occur in a matrix of coarse grained dolomite together with flakes of phlogopite and isolated grains of humite-group minerals and spinel. The magnetite occurs as subidiomorphic crystals and the spinel shows a greenish colour. Forsterite is present as an accessory mineral and is mostly transformed into serpentine (Fig. 3d).

Table 5. *Selected microprobe analyses of norbergite and chondrodite from the dolomite marbles; cations for norbergite are calculated on the basis of 5 oxygen atoms and for chondrodite on the basis of 10 oxygen atoms*

Mineral	Norbergite					Chondrodite				
Sample	920	920	920	908	908	909	909	909	909	920
Spot	4.10	4.11	4.12	5.2′	5.2″	1.1	1.2	1.4	3.12	2.22
SiO_2	28.35	28.40	28.35	29.29	29.61	33.16	33.20	33.27	32.96	32.85
TiO_2	0.07	0.09	0.00	0.02	0.06	0.55	0.20	0.36	0.32	0.07
Al_2O_3	0.00	0.00	0.00	0.00	0.00	0.00	0.00	0.00	0.02	0.01
FeO*	3.27	3.53	3.49	2.92	2.21	12.34	12.26	12.19	9.93	11.37
MnO	0.25	0.19	0.16	0.36	0.33	1.03	1.09	1.03	0.55	0.58
MgO	55.23	53.97	55.78	54.91	56.07	47.26	47.63	47.17	50.34	48.15
CaO	0.07	0.10	0.05	0.11	0.02	0.11	0.14	0.14	0.12	0.03
F	9.20	8.56	9.13	8.74	9.32	3.67	4.09	4.02	4.44	4.71
Total	96.44	94.84	96.96	96.35	97.62	98.13	98.60	98.18	98.72	97.76
Si	0.99	1.00	0.99	1.02	1.02	2.00	2.02	2.00	1.96	1.98
Ti	0.00	0.00	0.00	0.00	0.00	0.03	0.00	0.02	0.02	0.00
Al	0.00	0.00	0.00	0.00	0.00	0.00	0.00	0.00	0.00	0.00
Fe	0.09	0.10	0.10	0.08	0.06	0.68	0.70	0.69	0.57	0.66
Mn	0.00	0.00	0.00	0.01	0.01	0.05	0.05	0.05	0.03	0.03
Mg	2.89	2.86	2.90	2.85	2.88	4.24	3.43	4.25	4.42	4.33
Ca	0.00	0.00	0.00	0.00	0.00	0.00	0.00	0.00	0.00	0.00
Total	3.98	3.97	3.99	3.96	3.97	7.00	6.90	7.00	7.00	7.00
F	0.87	0.81	0.86	0.83	0.88	0.70	0.78	0.77	0.82	0.91
OH	1.12	1.16	1.14	1.13	1.08	1.24	1.17	1.20	1.17	1.10
X_{Mg}	0.97	0.97	0.97	0.97	0.98	0.96	0.83	0.92	0.97	0.90
X_F	0.44	0.41	0.43	0.42	0.45	0.36	0.40	0.39	0.41	0.45

* Total Fe = Fe^{2+}

Humite group minerals are difficult to distinguish from one another, but bearing in mind their general formulae $nM_2SiO_4M(OH, F)_2$ with M = Mg, Fe, etc. and n = 1, 2, 3 and 4 for norbergite, chondrodite, humite, and clinohumite, respectively, the analyzed minerals correspond to norbergite and chondrodite (Table 5). In the samples studied, the norbergite has $n \sim 1$ and X_F ranging from 0.40 to 0.45 and the chondrodite has $n \sim 2$ and X_F ranging from 0.36 to 0.45. On several occasions chondrodite appears as subhedral, more or less elongated crystals with a high relief which sometimes show marked yellowish pleochcroism and characteristic twinning. Norbergite has minor relief, low birefringence and no twins. The textural relationships between the two humites are not sufficiently clear to establish a genetic sequence. It is common to observe that chondrodite is transformed into norbergite but sometimes, as shown in Fig. 3e, the sequence seems to be in reverse.

The spinel-group minerals belong to the spinel-hercynite series (or ferrous spinel $MgAl_2O_4$–$FeAl_2O_4$) with an approximate formula of $Fe^{2+}_{0.49}Mg_{0.52}Fe^{3+}_{0.11}Al_{1.98}$. Phlogopite is not as abundant as in dolomite marbles without humites. The Mg/(Mg + Fe) ratio between 0.9 and 0.93 is similar to the phlogopite from the forster-

ite–diopside marbles, but the fluorine content is higher: $X_F = 0.33–0.42$ (Table 3, sample 908). Diopside, clintonite and amphibole are absent in these marbles. There is apatite and fluorapatite with 4.46 wt.% fluorine content. There are also pyrrothite, some chalcopyrite and occasionally arsenopyrite. Magnesian chlorite appears in these marbles as an alteration mineral. According to *Wiewióra* and *Weiss* (1990), its chemical composition, summarized in Table 4, ranges between clinochlore and pennine. X_F of the magnesian chlorites spans the range of 0.004–0.033.

The calcite marbles

The samples of the calcite marble protolith were collected at the Endrinal syncline (Fig. 1b). Compositionally and texturally these rocks are calcarenites of grey colour. The high quartz content and the grain size homogeneity gives calcarenites a compact aspect. There are fine grained whitish zones with archaeocyathides. These rocks contain 64.9–96% calcite, 2.5–21.9% quartz, 2.1–3.8% plagioclase, <1–13.5% phyllosilicates (phlogopite, muscovite and chlorite) and up to 7.9% dolomite. There are only minor amounts of sulphides (<1%) present. In metamorphic

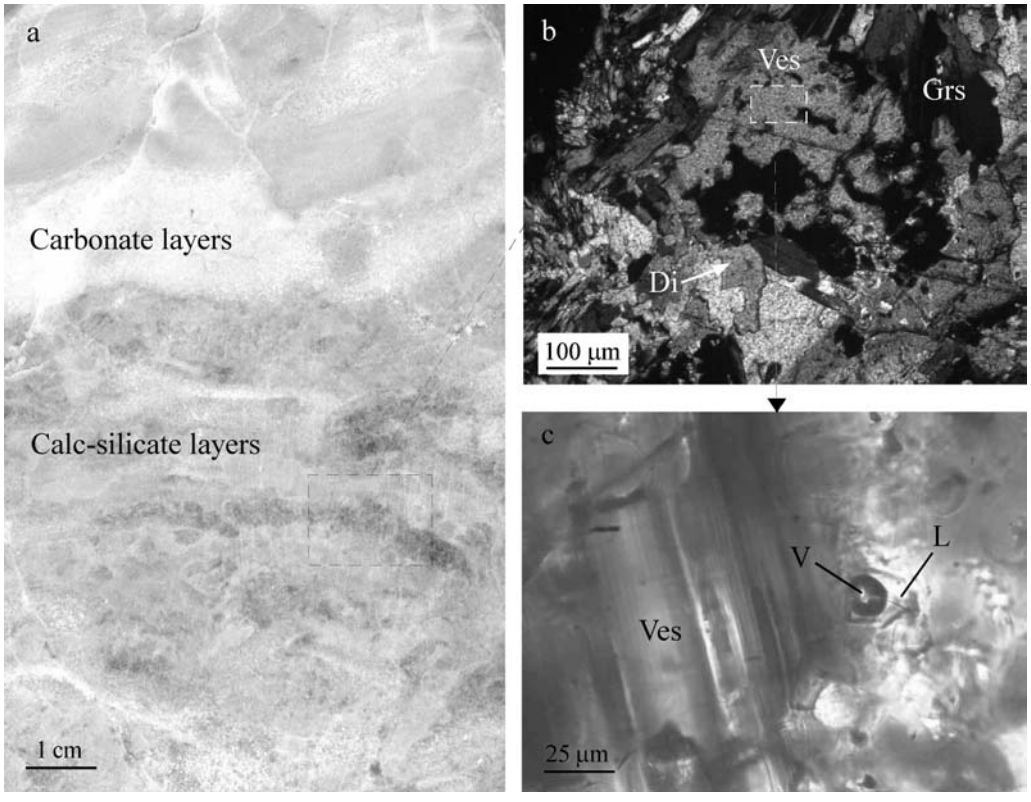

Fig. 4. (a) Portion of a calcite marble; light coloured layers contain predominantly calcite (Cal); calc-silicate layers have brown colour due to the presence of vesuvianite (Ves), or garnet (Grs), and greenish colour due to the presence of diopside (Di); (b) photomicrograph in transmitted light of grossular, diopside and calcite assemblage in vesuvianite; (c) two phase fluid inclusion in vesuvianite from Los Santos Este calcite marble

equivalents the texture varies from granoblastic to granolepidoblastic. Calcite grain size ranges from 70 to 100 µm. Sometimes they contain dolomite, which may become even more abundant than calcite. This dolomite is secondary in origin and it can appear as sparitic crystals, replacing fossil components or filling late

Table 6. *Compositions and mineral formulae of garnet (Grt), clinopyroxene (Di) and vesuvianite (Ves) from calcite marbles. Structural formulae of grossular on the basis of 12 oxygen atoms, clinopyroxene on the basis of 6 oxygens atoms, and vesuvianite on the basis of 78 oxygens atoms; Fe^{3+} is estimated following stoichiometric constrains for Di and Grt and following* Groat *et al. (1992) for Ves*

Mineral	Grt	Di		Ves
Sample	960	960	960	960
Spot	1.59	2.54	1.60	4.61
SiO_2	39.01	53.27	52.44	36.03
TiO_2	0.43	0.06	0.04	1.27
Al_2O_3	19.62	1.07	0.86	16.41
Fe_2O_3*	3.67	0.00	0.00	–
FeO	0.00	5.65	4.48	2.29
MnO	0.21	0.07	0.09	0.05
MgO	0.48	13.36	14.54	2.62
CaO	36.02	26.34	25.85	36.42
Na_2O	0.03	0.07	0.04	0.03
K_2O	0.01	0.00	0.01	0.00
F	–	–	–	0.01
Cl	–	–	–	0.23
Total	99.48	99.90	98.34	95.38
Si	2.98	1.98	1.97	17.21
Ti	0.02	0.00	0.00	0.46
Al	1.77	0.05	0.04	9.24
Fe^{3+}*	0.21	0.00	0.00	1.35
Fe^{2+}	0.00	0.18	0.14	0.91
Mn	0.01	0.00	0.00	0.02
Mg	0.06	0.74	0.81	1.87
Ca	2.95	1.05	1.04	18.64
Na	0.00	0.00	0.00	0.03
K	0.00	0.00	0.00	0.00
F	0.00	0.00	0.00	0.02
Cl	0.00	0.00	0.00	0.19
Total	8.01	3.99	4.01	49.72
		X_{Mg} 0.81	0.85	0.67
Alm	0.01	Di 80.60	85.00	
Adr	10.52	Hd 19.40	15.00	
Grs	87.19	Jh 0.00	0.00	
Prp	1.95			
Sps	0.33			

* Recalculated from stoichiometry

microfractures. A light layering is defined by preferred orientation of micas, mainly phlogopite, muscovite, and chlorite. In some samples, together with calcite, sericite is an essential component. Common accessory minerals are tourmaline and opaque minerals. Disseminated euhedral pyrite cubes are found all over the sample but, frequently, oriented accumulations of pyrite accompanied by ferric oxides in very fine grained layers are also observed.

The contact metamorphism of the calcic marbles has resulted in the appearance of diopside, grossular, and vesuvianite with or without wollastonite. Table 1 summarises the most important minerals in these marbles.

Diopside–grossular–vesuvianite ± wollastonite marbles. These rocks are coarse-grained and show banding on a millimetre to centimetre scale. Whitish bands represent carbonate-rich and/or wollastonite rich layers. Greenish bands consist of clinopyroxene and the brownish bands contain vesuvianite and grossular (Fig. 4a). Mineral assemblages in these rocks are dependent on the initial composition of the individual layers in which they occur. In calcite-rich layers, the calcite is coarse grained (300–600 μm) and granoblastic. Mineral assemblages in calc-silicate layers, contain calcite, diopside, grossular, vesuvianite and wollastonite. The diopside, grossular and calcite association occurs as relicts. Diopside occurs as subhedral grains (<50 μm). Garnet is fine grained and anhedral. Whenever vesuvianite is present it replaces garnet (Fig. 4b). Wollastonite appears as fine needles with calcite and diopside inclusions. Vesuvianite is very abundant and contains all of the minerals mentioned above. Sometimes up to centimetre-sized porphyroblasts of vesuvianite occur at the boundary between calc-silicate layers and calcite-rich layers.

From chemical analyses, the garnet can be classified as grossular (Table 6). The clinopyroxene is essentially a diopside-hedenbergitic solid solution ($Di_{0.80–0.85}$; $Hd_{0.15–0.19}$) (Table 6). The vesuvianite has a F content of 0.02 wt.% (Table 6). In contrast all phases which are present as inclusions in vesuvianite (primary calcite, diopside and grossular) are F free.

Phase relations

Hornfelses. The mineral association produced during contact metamorphism of the hornfelses consists of cordierite, K-feldspar, andalusite and locally, sillimanite with quartz, moscovite, excess biotite and ilmenite. This assemblage may be considered in the simplified $K_2O–FeO–MgO–Al_2O_3–SiO_2–H_2O$ model system (KFMASH). Phase relations within this system were calculated using the internally consistent thermodynamic database of *Berman* (1988) with the aid of the Geo-Calc software (*Berman* et al., 1987; *Brown* et al., 1988a, b). A phase diagram projection was constructed for the hornfelses using unit activity for quartz, andalusite, sillimanite and kyanite because they occur as pure phases. Activities of the rest of the minerals were corrected using models from published experiments: for moscovite and biotite, those from *Essene* (1989), for K-feldspar, the model proposed by *Spear* (1993), and for cordierite, the model reported by *Powell* and *Holland* (1990) were used. Figure 5 shows the phase relations in a *P–T* diagram. The prograde reaction in the metapelites are characterized by the breakdown of muscovite and quartz to give K-feldspar and andalusite (R1) before andalusite converts to sillimanite (R2).

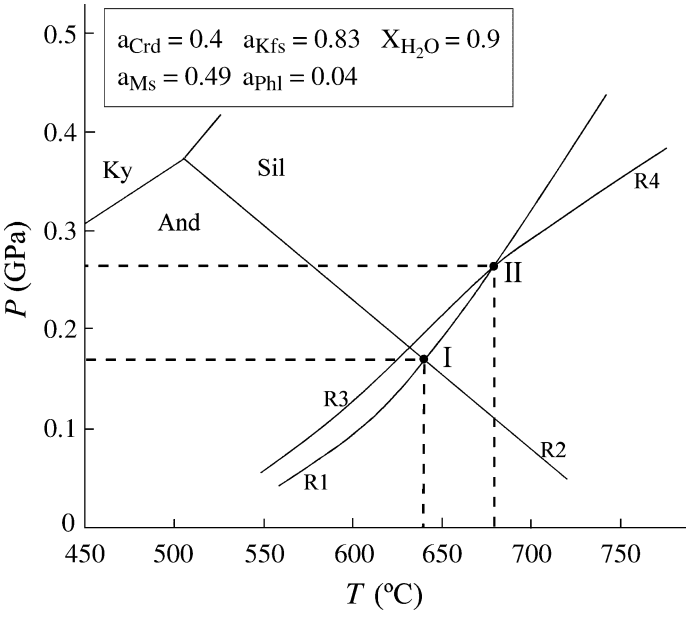

Fig. 5. P–T projection of the K_2O–FeO–MgO–Al_2O_3–SiO_2–H_2O system. The position of the reactions R1, R3 and R4 have been corrected according to mineral compositions: $a_{Mg-Crd} = 0.4$, $a_{Kfs} = 0.83$, $a_{Ms} = 0.49$ and $a_{Phl} = 0.04$. For the rest of mineral phases, activity is equal to unity

This reaction sequence indicates that prograde reaction took place at pressures below 0.17 GPa. These reactions intersect at point I ($P = 0.17$ GPa; $T = 640$ °C):

$$\text{muscovite} + \text{quartz} = Al_2SiO_5 + \text{K-feldspar} + H_2O \quad \text{(R1)}$$

$$\text{andalusite} = \text{sillimanite} \quad \text{(R2)}$$

The development of assemblages such as cordierite, andalusite and K-feldspar, suggest that reactions R3 and R4 occurred, which intersect at point II ($P = 0.26$ GPa; $T = 680$ °C).

$$6\ \text{moscovite} + 2\ \text{biotite} + 15\ \text{quartz} = 3\ \text{cordierite} + 8\ \text{K-feldspar} + 8\ H_2O \quad \text{(R3)}$$

$$2\ \text{biotite} + 9\ \text{quartz} + 6\ Al_2SiO_5 = 3\ \text{cordierite} + 2\ \text{K-feldspar} + 2\ H_2O \quad \text{(R4)}$$

The Crd + And + Kfs assemblage containing sillimanite suggests that the P–T conditions in the Los Santos aureole are located between points I and II. Therefore, for the metapelites maximum temperature-pressure conditions of contact metamorphism are estimated between 640–680 °C and 0.18–0.27 GPa. This is in line with the findings of *Ugidos* (1987), who inferred temperatures of between 600 and 640 °C and pressures between 0.2 and 0.25 GPa for contact metamorphism in the Spanish central western zone.

Dolomite marbles. Mineral assemblages and their chemical compositions must be considered in terms of the components K_2O, CaO, MgO, Al_2O_3, SiO_2, H_2O and CO_2. Phase relations within this system were calculated using the internally consistent thermodynamic database of *Berman* (1988) with the aid of the Geo-Calc software (*Berman* et al., 1987; *Brown* et al., 1988a, b). A phase diagram projection was constructed for the forsterite-diopside-phlogopite marbles using unit activity

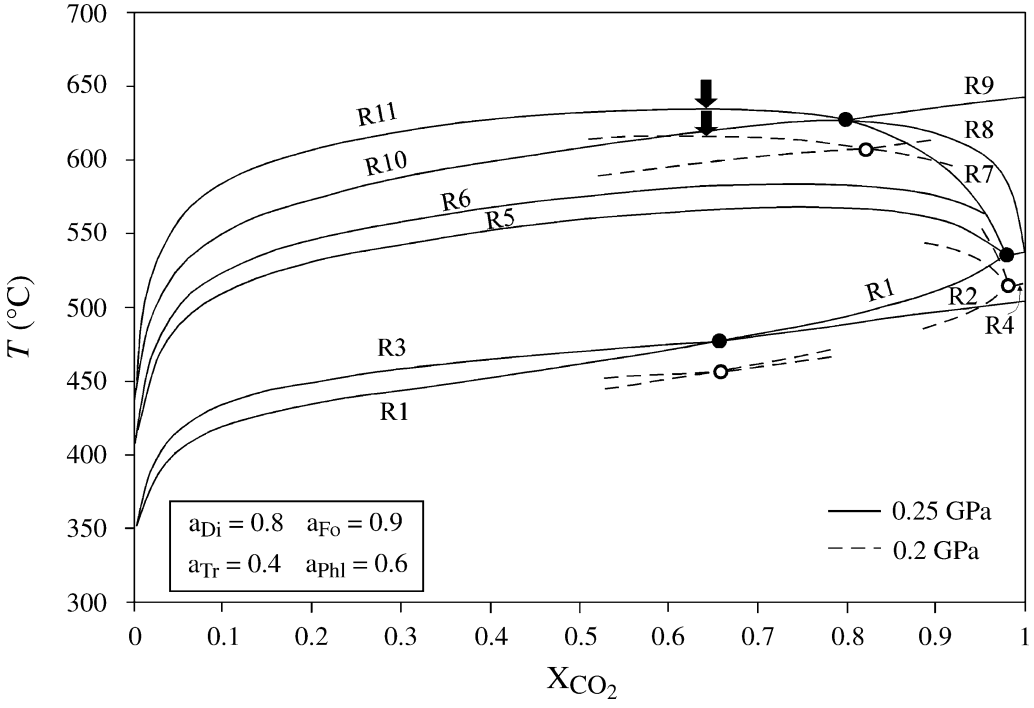

Fig. 6. T–X_{CO_2} phase diagram summarizing reactions in the K_2O–CaO–MgO–Al_2O_3–SiO_2–H_2O–CO_2 system at 0.25 GPa (continuous curves) and at 0.2 GPa (discontinuous curves). The arrows represent the maximum conditions of T and X_{CO_2} for the reaction that reflects the most common assemblage in the dolomitic marbles (forsterite-diopside-phlogopite). The numbered reactions are as follows:

$$8\,\mathrm{Qzt} + 5\,\mathrm{Dol} + \mathrm{H_2O} = 3\,\mathrm{Cal} + \mathrm{Tr} + 7\,\mathrm{CO_2} \quad \text{(R1)}$$

$$2\,\mathrm{Dol} + \mathrm{Phl} + 8\,\mathrm{Qzt} = \mathrm{Tr} + \mathrm{Kfs} + 4\,\mathrm{CO_2} \quad \text{(R2)}$$

$$6\,\mathrm{Cal} + 5\,\mathrm{Phl} + 24\,\mathrm{Qzt} = 3\,\mathrm{Tr} + 5\,\mathrm{Kfs} + 2\,\mathrm{H_2O} + 6\,\mathrm{CO_2} \quad \text{(R3)}$$

$$\mathrm{Dol} + 2\,\mathrm{Qzt} = \mathrm{Di} + 2\,\mathrm{CO_2} \quad \text{(R4)}$$

$$3\,\mathrm{Cal} + 2\,\mathrm{Qzt} + \mathrm{Tr} = 5\,\mathrm{Di} + \mathrm{H_2O} + 3\,\mathrm{CO_2} \quad \text{(R5)}$$

$$3\,\mathrm{Tr} + \mathrm{Kfs} + 6\,\mathrm{Cal} = 12\,\mathrm{Di} + \mathrm{Phl} + 6\,\mathrm{CO_2} + 2\,\mathrm{H_2O} \quad \text{(R6)}$$

$$3\,\mathrm{Cal} + \mathrm{Tr} = \mathrm{Dol} + 4\,\mathrm{Di} + \mathrm{H_2O} + \mathrm{CO_2} \quad \text{(R7)}$$

$$5\,\mathrm{Dol} + 4\,\mathrm{Tr} = 6\,\mathrm{Fo} + 13\,\mathrm{Di} + 4\,\mathrm{H_2O} + 10\,\mathrm{CO_2} \quad \text{(R8)}$$

$$4\,\mathrm{Cal} + 2\,\mathrm{Fo} + 2\,\mathrm{CO_2} = 3\,\mathrm{Dol} + \mathrm{Di} \quad \text{(R9)}$$

$$13\,\mathrm{Cal} + 8\,\mathrm{Fo} + 9\,\mathrm{CO_2} + \mathrm{H_2O} = \mathrm{Tr} + 11\,\mathrm{Dol} \quad \text{(R10)}$$

$$5\,\mathrm{Cal} + 3\,\mathrm{Tr} = 2\,\mathrm{Fo} + 11\,\mathrm{Di} + 3\,\mathrm{H_2O} + 5\,\mathrm{CO_2} \quad \text{(R11)}$$

for quartz, calcite, dolomite and K-feldspar, because they occur as nearly pure phases. Activities of diopside and forsterite were calculated according to *Spear* (1993). Tremolite was modelled after *Chernosky* et al. (1998); and for phlog-

opite the model of *Essene* (1989) was used. Figure 6 shows the phase relations in a T–X_{CO_2} diagram. According to the pressures obtained from the mineral assemblages in hornfelses, curves have been constructed at 0.25 and at 0.2 GPa.

The most common paragenesis observed in *forsterite–diopside–phlogopite marbles*, suggests that forsterite was formed by reaction R11:

$$5\ \text{calcite} + 3\ \text{tremolite} = 2\ \text{forsterite} + 11\ \text{diopside} + 3\ H_2O + 5\ CO_2 \quad \text{(R11)}$$

The maximum temperature of forsterite formation during contact metamorphism was estimated at 525 °C at 0.05 GPa, 570 °C at 0.1 GPa and 675 °C at 0.3 GPa (*Ferry*, 2001). For the Notch Peak (Utah) aureole, under similar metamorphic conditions, the temperature of forsterite formation is 590–600 °C at $P = 0.2$ GPa (*Hover-Granath* et al., 1983). *Bowman* and *Essene* (1982) calculated the low-T limit for this association between 500 and 550 °C. For the Los Santos aureole, R11 indicates a maximum temperature of 640 °C and $X_{CO_2} = 0.65$ at 0.25 GPa or at 610 °C and $X_{CO_2} = 0.62$ at 0.2 GPa (Fig. 6).

As described previously, clintonite can appear occasionally in dolomitic marbles at Los Santos Este. *Olesh* and *Seifert* (1976) determined the phase relations of clintonite in the system CaO–MgO–Al_2O_3–SiO_2–H_2O at 0.2 GPa and they established that the typical conditions for the formation of natural clintonites can be estimated to be 600–800 °C and about 0.2 GPa with X_{CO_2} ranging from 0.1 to 0.3. Clintonite is, hence, restricted to low X_{CO_2} values of the coexisting fluid. During contact metamorphism, the CO_2-rich phase of a carbonate rock might be diluted by penetrating H_2O solutions stabilizing clintonite. In addition, bulk compositions high in Al_2O_3 but low in SiO_2 are a prerequisite for clintonite formation. Such compositions led *Olesh* and *Seifert* (op. cit.) to suggest that clintonite will not form unless the original bulk composition is changed through metasomatism. On the other hand, *Rice* (1979) suggests that these special bulk-compositional requirements can be met in the original sediment and formation of clintonite was not necessarily related to metasomatism, but rather to nearly isochemical reactions taking place in H_2O-rich fluids. In the zone studied, MgSi-rich clintonite coexists with forsterite and chlorite. As stated previously, this association can be formed at between 600 and 660 °C. At higher temperatures chlorite will disappear.

In these less common bulk compositions the calcic amphibole (pargasite) also appears. From the crystals of diopside with inclusions of amphibole grains in optical continuity, it can be deduced that clinopyroxene was formed at the expense of pargasite and calcite.

Another mineral assemblage in the dolomitic marbles is characterized by the presence of calcite, dolomite, forsterite, chondrodite, norbergite, and spinel. Phlogopite is less abundant than in medium grade marbles. Diopside is absent, indicating low silica activity. *Rice* (1980a, b) constructed phase diagrams for the humite-group minerals. According to *Rice* (1980a, b), humites form when marbles containing the assemblage Cal–Dol–Fo–Spl–Phl are not capable of buffering the fluid composition from the equilibrium

$$\text{dolomite} + 4\ \text{forsterite} + H_2O = \text{clinohumite} + \text{calcite} + \text{quartz}$$

Formation of humites is favoured by low silica activity and by high HF fugacity in the fluid. The stability field for humites is primarily governed by this reaction, which has positive slopes in the T–X_{CO_2} space. Hence, an increase in temperature or a decrease in X_{CO_2} is necessary to replace forsterite by humite-group minerals. At 600 °C and 0.2 GPa the mole fraction of carbon dioxide in the fluid coexisting with the chondrodite-forsterite association is between 0.4 and 0.5 (*Rice*, 1980a, b).

In some samples, there are intergrowths of chondrodite and tremolite (Fig. 3f) suggesting the reaction

$$52 \text{ forsterite} + 2 \text{ calcite} + 12\ H_2O = 11 \text{ chondrodite} + \text{tremolite} + CO_2$$

An increase in temperature or a decrease in X_{CO_2} is required in order to allow this reaction to occur. According to *Rice* (1980b) and *Satish-Kumar* et al. (2001) temperature limits for this reaction range between about 630 and 575 °C and X_{CO_2} values between 0.65 and 0.35. In addition to chondrodite, these samples contain norbergite. It is difficult to define the textural relationships between the two humite group minerals. Sometimes it seems that chondrodite gives rise to norbergite (Fig. 3e) and at other times the norbergite seems to be unstable and prone to transformation to chondrodite. The equilibrium between the two minerals could be defined by a chemical reaction such as

$$\text{dolomite} + \text{chondrodite} + H_2O = 2 \text{ norbergite} + \text{calcite} + CO_2$$

Several authors have demonstrated that the increase in the stoichiometric quantity of (OH, F) in the humite series from clinohumite to norbergite is accompanied by an increase in the mole fraction of fluorine. This suggests that the relative rarity of chondrodite, and especially norbergite, is, at least in part, due to the lack of bulk compositions with suitably high $F/(F + OH)$ ratios.

In order to obtain more information about the thermal conditions during the contact metamorphism, calcite–dolomite solvus geothermometry has been used (*Anovitz* and *Essene*, 1987). According to these authors the limits to apply this geothermometer range from 250 to 800 °C with uncertainties of ±50 °C when T is less than 500 °C and ±25 °C when T is above 500 °C. Calcite–dolomite geothermometry has been applied to humite and spinel-bearing assemblages and most of the temperatures obtained (seven measurements) range between 514 and 355 °C (±25 °C).

Calcite marbles

Many studies indicate that parageneses with vesuvianite are restricted to water rich fluids (*Valley* et al., 1985; *Labotka* et al., 1988; *Abart*, 1995). In a qualitative analysis of reactions in the CaO–MgO–Al_2O_3–SiO_2–H_2O–CO_2 system *Valley* et al. (1985) show that assemblages with vesuvianite are stable to high temperatures in the absence of quartz and require water-rich conditions ($X_{H_2O} > 0.8$). In the calcic marbles studied, the garnet is rimmed and replaced by vesuvianite, which contains many diopside and calcite inclusions. These observations suggest that vesuvianite may have been formed by the reaction

$$2 \text{ grossular} + 3 \text{ diopside} + 3 \text{ anorthite} + 7 \text{ calcite} + 4\ H_2O = \text{vesuvianite} + 7\ CO_2$$

Other samples contain wollastonite that could have been formed according to the reaction

$$\text{calcite} + \text{quartz} = \text{wollastonite} + CO_2$$

In these samples the vesuvianite grains either contain wollastonite inclusions or are intergrown with wollastonite blades suggesting that vesuvianite may have been formed at the expense of grossular within the stability field of wollastonite by the reaction

$$5\ \text{garnet} + 3\ \text{diopside} + 4\ \text{calcite} + 4\ H_2O = \text{vesuvianite} + 3\ \text{wollastonite} + 4\ CO_2$$

According to the authors mentioned above, in the presence of wollastonite, vesuvianite requires very water-rich conditions ($X_{H_2O} > 0.97$) and temperatures higher than 600 °C.

Fluid inclusions

In calcic marbles, fluid inclusions suitable for analysis were found in vesuvianite. Within vesuvianite, single, equant and isolated fluid inclusions are distributed randomly in individual grains and are interpreted to be primary inclusions (*Roedder*, 1984). These fluid inclusions are two-phase inclusions consisting of a gas bubble (V) surrounded by an aqueous liquid (L), where V > L. According to the fluid content at room temperature the degree of filling is 0.6 (*Roedder*, 1984). The liquid is an aqueous saline fluid and the gaseous phase is a gaseous mixture. These fluid inclusions vary in size from 8 to 40 μm and show ovoidal, irregular, elongated and polygonal shape (Fig. 4c).

Microthermometric data

On cooling, the inclusions exhibit freezing, with initial clathrate formation followed by ice formation at lower temperatures, which results in a distortion of the

Table 7. *Summary of fluid inclusion data for vesuvianite at Los Santos*

Host mineral	vesuvianite
Type of fluid inclusion	L + V (V > L)
No. of measurements	20
T_{mCO_2}	−60 to −61
T_e	−52.7 to −22
T_{mice}	−11 to −9.8
T_{mclath}	8 to 9.8
T_h	403 to 411
Salinity (wt.% NaCl equiv.)	7.6 to 9.53
Density (g/cm^3)	0.66
X_{CO_2}	0.05
X_{H_2O}	0.9
X_{NaCl}	0.05

T_{mCO_2} Triple point CO_2, T_e eutectic temperature, T_{mice} melting ice, T_{mclath} melting clathtrate, T_h homogeneization temperature

vapour phase. Phase transitions in these gaseous inclusions were observed between −170 and +20 °C, a temperature range that can be investigated by cooling the sample with liquid N_2. All the data obtained are summarised in Table 7. Complete solidification of these inclusions was not observed but, on warming runs, the initial melting of the fluid inclusions in vesuvianite from Los Santos Sur were observed between −61 and −60 °C. This melting occurs far from the triple point of pure CO_2 at −56.6 °C. According to *Van den Kerkhof* and *Thiéry* (2001) additional components such as CH_4 or N_2 will lower the melting temperature down to −61 °C for CO_2–N_2 mixtures and down to much lower temperatures for CO_2–CH_4. So, probably, the gaseous phase of these fluid inclusions contains a mixture of CO_2 and N_2. However, the presence of CH_4 should not be discarded because the clathrate melting temperature is nearly 10 °C (*Sheperd* et al., 1985).

In the aqueous phase, the first melting of the inclusions in vesuvianite is observed between −52.7 and −22 °C, indicating not only the presence of Na^+ but also of minor amounts of cations such as Ca^{2+} or Mg^{2+} (*Sheperd* et al., 1985). The final melting of ice takes places between −11 and −9.8 °C and the final melting temperature of the clathrates ranges from 7.6 to 9.8 °C. From this data and using Ice program (*Bakker*, 1999) the salinity and density have been estimated to be 8.7 wt.% NaCl equiv. and 0.62 g/cm^3 respectively, and the CO_2 molar fraction is estimated to be $X_{CO_2} \sim 0.05$. Total homogenization temperatures vary between 403 and 411 °C, and the homogenization is always to the liquid. The isochores were calculated from the volume and composition properties of the fluid using the Isochor program (*Bakker*, 1999). The trapping temperatures estimated for inclusions in vesuvianite, corrected for a trapping pressure between 0.2 and 0.25 GPa ranges between 548 and 618 °C.

The fluid inclusions of vesuvianite do not contain evidence of boiling, because they are identical in appearance, composition, density, and, there are no different coexisting fluid inclusions, which homogenize into both liquid and vapour phases at similar temperatures.

Fluid–rock interaction

Carbon and oxygen isotope compositions of carbonates

The isotopic composition of a metamorphic rock is controlled by (1) the composition of the protolith; (2) the effects of devolatilization; (3) exchange with infiltrating fluids; and (4) the temperature of exchange (*Valley*, 1986). The isotopic composition of dolomite in unaltered dolostone and of calcite in dolomite and calcite marbles are shown in Fig. 7a. Dolomite from the unaltered Cambrian marbles shows an average of $\delta^{13}C_{PDB} = -1.52‰$ and $\delta^{18}O_{SMOW} = 20.79‰$, typical isotopic composition for marine carbonates of Cambrian age (*Veizer* and *Hoefs*, 1976). $\delta^{18}O$ values of calcite from calcite and dolomite marbles vary from 11.68 to 14.41‰ and the $\delta^{13}C$ values vary from −6.42 to −3.10‰ (Fig. 7a).

The calcites from marbles are depleted in both ^{13}C and ^{18}O relative to the unaltered dolostone (see Fig. 7a). The pattern of depletion in both isotopes is consistent with many contact aureoles and in general, with most of the skarns world wide (*Valley*, 1986). In any event, depletions can be attributed to the decarbonation

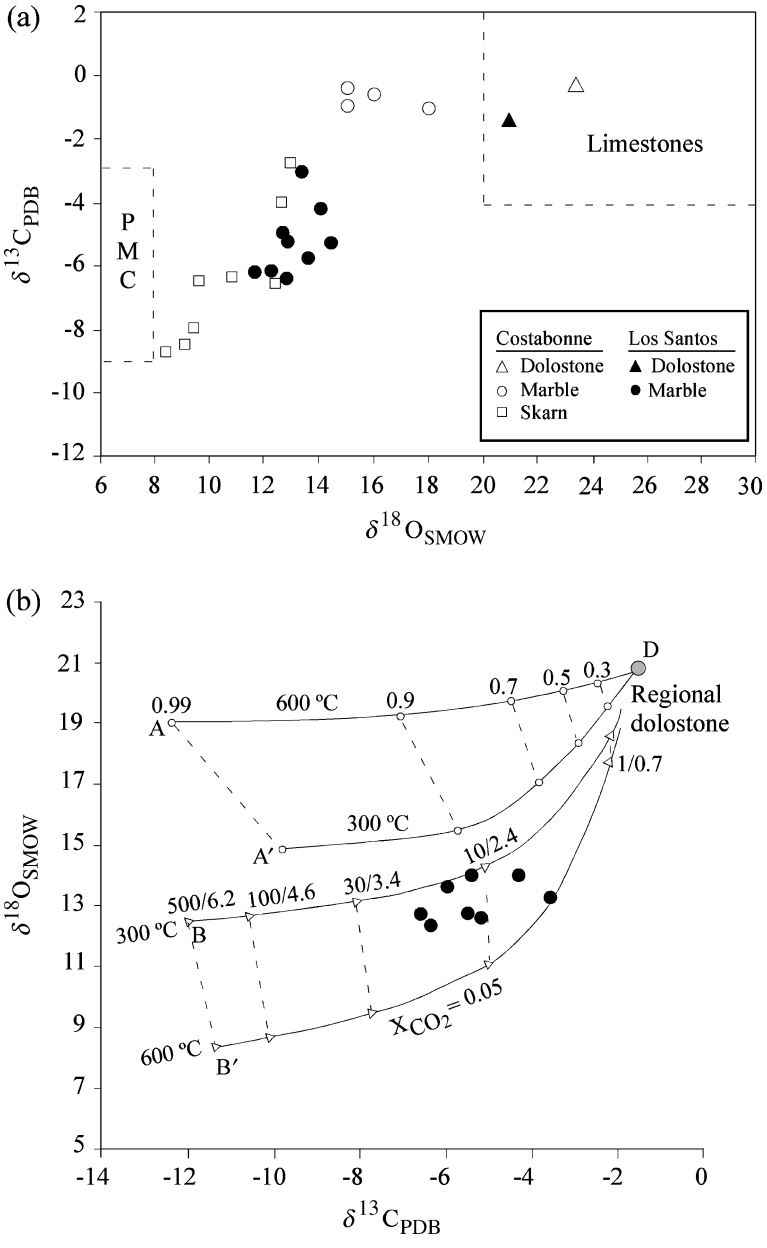

Fig. 7. (a) Plot of $\delta^{13}C$ versus $\delta^{18}O$ for calcite from Los Santos and regional dolostone; the Costabonne data are from *Guy* et al. (1988); the areas for limestone and for primary carbon (PMC) are given for reference; (b) plot of $\delta^{18}O$ versus $\delta^{13}C$ values for calcites of the marbles (solid circles) from Los Santos. Curves D–A and D–A′ correspond to a Rayleigh type carbonate devolatilization between 300 and 600 °C, taking as initial rock composition $\delta^{18}O = 20.79$ and $\delta^{13}C = -1.52$ per mil. Curves D–B and D–B′ correspond to an exchange mechanism between that composition and a fluid with $\delta^{18}O = 6.63$ and $\delta^{13}C = -14.19$ per mil at 300 and 600 °C. X_{CO_2} in the hydrothermal fluid has been assumed as 0.05. Numbers from 1 to 500 are the fluid/rock ratios in a closed system and the ones from 0.7 to 6.2 in an open system. Numbers between 0.3 and 0.99 are the factor of the devolatilization Rayleigh

phenomena, both in contact metamorphosed marbles (*Lattanzi* et al., 1980) and in skarns (*Shieh* and *Taylor*, 1969). Alternatively depletion in ^{13}C could be attributed to the incorporation of isotopically light carbon derived from the quantitative oxidation of graphite by a metasomatic fluid (*Abart*, 1995).

In order to ascertain whether the depletion observed in samples from Los Santos is due to decarbonation processes or to exchange with a metasomatic fluid, a simulation of depletions produced by either one of these processes has been performed. The carbon isotope composition of the carbonates reflects the degree of development of these processes. The oxygen isotope composition is controlled by interaction with a hydrothermal fluid and temperature (*Valley*, 1986). The effects of devolatilization can be modelled as one of two end-member processes: batch devolatilization, where all the fluid equilibrates with the rock before leaving the system; and Rayleigh distillation, where the volatile species are continuously isolated from their origin due to steady fluid expulsion (*Valley*, op. cit).

In order to calculate the curves representing Rayleigh distillation for carbon the equation of *Bowman* et al. (1985) has been used:

$$\delta^{13}C_{cal(f)} = (\delta^{13}C_{CO_2(i)} + 1000) * F^{((\alpha CO_2 - cal)-1)} - 1000$$

where $\delta^{13}C_{cal(f)}$ is the isotopic composition of the calcite after decarbonation, and $\delta^{13}C_{CO_2(i)}$ is the initial isotopic composition of the fluid. F is the mole fraction of C remaining in the system after decarbonation. The isotopic fractionation between CO_2 and calcite was calculated from the equations of *Bottinga* (1969) for each $T(\alpha_{CO_2-cal})$. The final $\delta^{18}O$ of the calcite was calculated using the analogous equation:

$$\delta^{18}O_{cal(f)} = (\delta^{18}O_{H_2O(i)} + 1000) * F^{((\alpha H_2O - cal)-1)} - 1000$$

with similar meanings of the variables. The isotope fractionation factor between calcite and water (α_{H_2O-cal}) was calculated from the equations of *Zheng* (1999) for a given temperature. In order to calculate the mole fraction of O at each stage, the decarbonation reaction specified has to be considered (*Bowman* et al., 1985).

In order to calculate the final isotopic composition of the calcite for a batch volatilization process the following equations were used (*Bowman* et al., 1985).

$$\delta^{13}C_{cal(f)} = X_{CO_2} * \Delta_{cal-CO_2} + \delta^{13}C_{cal(i)}$$

$$\delta^{18}O_{cal(f)} = X_{O_2} * \Delta_{rock-CO_2} + \delta^{18}O_{cal(i)}$$

$\delta^{13}C_{cal(i)}$ and $\delta^{18}O_{cal(i)}$ are the initial carbon and oxygen isotope compositions of calcite, $\delta^{13}C_{cal(f)}$ and $\delta^{18}O_{cal(f)}$ are the carbon and oxygen isotope compositions of the fluid, and Δ_{cal-CO_2} is the calcite-CO_2 fractionation, X_{O_2} is the number of moles of oxygen involved in each decarbonation stage. The isotopic effects of devolatilization were calculated for the reaction of diopside, $CaMg(CO_3)_2 + 2\,SiO_2 = CaMgSi_2O_6 + 2\,CO_2$, at temperatures between 300 and 600 °C.

Batch devolatilization produces significant depletions both in ^{13}C and ^{18}O. Rayleigh distillation produces depletions in ^{13}C similar to those of the samples studied, but it does not explain depletions in ^{18}O (Fig. 7b). To explain the depletion in ^{13}C and ^{18}O observed it is necessary to invoke isotopic exchange between a CO_2 bearing metasomatic fluid and the rock. In this case the isotopic composition of the resulting calcite depends on the following factors: the initial composition of the fluid

($\delta^{13}C_{CO_2}$ and $\delta^{18}O_{H_2O}$), the isotopic composition of the unaltered limestone, the temperature and the water-rock ratio. We applied this model to simulate the effects of carbon and oxygen isotope exchange between unaltered dolomite, with $\delta^{13}C = -1.52$ and $\delta^{18}O = 20.79‰$ and a metasomatic fluid with $\delta^{13}C = -14.19$ and $\delta^{18}O = 6.63‰$ at temperatures between 300 and 600 °C and X_{CO_2} between 0.01 and 0.5. The X_{CO_2} has been chosen taking into account the study of the mineral phases and of the fluid inclusions. The choice of the isotope values of the fluid phase was made in accordance with the isotopic composition of the isotopically light hydrothermal calcite analysed. This calcite belongs to an amphibole skarn of the Santos Sur sector.

The curve for oxygen isotope exchange of calcite can be calculated from the mass balance equation (*Taylor*, 1974):

$$W/R = n * [(\delta^{18}O_{cal(f)} - \delta^{18}O_{cal(i)})/(\Delta^{18}O_{cal-H_2O} + \delta^{18}O_{H_2O(i)} - \delta^{18}O_{cal(f)})]$$

$\delta^{18}O_{cal(f)}$ is the oxygen isotope composition of the calcite after exchange, $\delta^{18}O_{cal(i)}$ is the initial oxygen isotope composition of calcite, $\delta^{18}O_{H_2O(i)}$ is the initial oxygen isotope composition of the metasomatic fluid, and $\Delta^{18}O_{cal-H_2O}$ expresses the oxygen isotope fractionation between calcite and fluid. W/R is the water/rock ratio. As the calcite has three moles of oxygen, n will be 3. The oxygen isotope composition of calcite can be expressed as a function of the water-rock ratio by:

$$\delta^{18}O_{cal(f)} = [(W/3R) * \Delta^{18}O_{cal-H_2O} + (W/3R) * \delta^{18}O_{H_2O(i)} + \delta^{18}O_{cal(i)}]/[1 + (W/3R)]$$

The isotope exchange curve for carbon can be calculated using the analogous equation:

$$W/R = nc/X_{CO_2} * [(\delta^{13}C_{cal(f)} - \delta^{13}C_{cal(i)})/(\Delta^{13}C_{cal-CO_2} + \delta^{13}C_{CO_2(i)} - \delta^{13}C_{cal(f)})]$$

where $nc = 1$ is the number of moles of C per mole of calcite and the other parameters have similar meanings as in the analogous expression for the oxygen system. Clearing $\delta^{13}C_{cal(f)}$ we obtain:

$$\delta^{13}C_{cal(f)} = [(W/R) * X_{CO_2} * \Delta^{13}C_{cal-CO_2} + (W/R) * X_{CO_2} * \delta^{13}C_{CO_2} + \delta^{13}C_{cal(i)}]/[1 + (W/R) * X_{CO_2}]$$

which expresses that the final composition of the calcite depends on the mole fraction of CO_2 in the fluid. The final theoretical composition of the calcite for different water/rock ratios and X_{CO_2} values can be calculated using this relationship.

If the isotope exchange occurs in an open system the isotope exchange curve can be re-calculated using the relation (*Taylor*, 1977):

$$(W/R)o = \ln[(W/R)c + 1]$$

(W/R)o and (W/R)c are the water/rock ratios in an open and closed-system, respectively. This way, under the same conditions of *T*, X_{CO_2} and initial isotope compositions of the fluid and the rock, the amount of fluid necessary to obtain a certain depletion will be smaller if the system is open than if it is closed.

From the comparison of data and calculations (Fig. 7) it is inferred that the curves of isotope exchange reflect the progressive ^{18}O and ^{13}C depletion. Figure 7b

illustrates how the ^{18}O and ^{13}C depletion could correspond to an isotope exchange between carbonate and a fluid. The curve of the isotope exchange generated from a fluid with $\delta^{13}C = -14.19$, $\delta^{18}O = 6.63‰$ and $X_{CO_2} = 0.05$ and a carbonate rock with $\delta^{13}C = -1.52$ and $\delta^{18}O = 20.79‰$, at temperatures ranging from 600 to 300 °C and with fluid/rock ratios between 2.4 and 3.4 in an open system could serve as a model for the evolution of calcites analysed (Fig. 7b, curves D–B and D–B′).

F metasomatism

The humite group minerals can appear in metamorphosed impure carbonate rocks, during the low-pressure contact metamorphism and metasomatism, involving the introduction of fluorine and reaction with pre-existing silicates (*Piazolo* and *Markl*, 1999). Other authors, on the other hand, point out that humites also form in regionally metamorphosed zones not spatially related to an igneous body, by isochemical reactions involving (OH–F) silicates, such as calcic amphibole, chlorite, phlogopite, and H_2O–CO_2-rich fluids (*Moore* and *Kerrick*, 1976; *Rice*, 1977; *Valley* et al., 1982). The study of the humites from Los Santos supports the first hypothesis but not the second. *Rice* (1980a, b) argues that the prograde sequence clinohumite → chondrodite → norbergite is inconsistent with the isochemical model. He suggests that the formation of norbergite results from metasomatic introduction of fluorine into the system after the formation of clinohumite and/or chondrodite. Norbergite formation requires high fluorine content and, if a high ratio of $F/(F + OH)$ is already present in the protolith, norbergite will form first (*Rice*, 1980b). The order of preference of F relative to OH is: norbergite $X_F = 0.45$ > chondrodite $X_F = 0.41$ > phlogopite $X_F = 0.08$ > clintonite $X_F = 0.05$ > pargasite $X_F = 0.045$ > chlorite $X_F = 0.0108$ (Tables 3–5). This sequence of partitioning of fluorine during prograde metamorphism is in accordance with that described by *Rice* (1980a) (clinohumite > phlogopite > tremolite > chlorite).

The external influx of an aqueous fluid is also evident because of the vesuvianite–wollastonite association in calcite marble. In closed, H_2O-rich, siliceous marble systems, wollastonite begins to form at 600 °C, and may continue to grow at temperatures as high as 700 °C at 0.2 GPa in dolomite-bearing systems (*Bucher* and *Frey*, 1994). In contact aureoles the wollastonite-forming reaction may be driven by infiltration of silica and calcite rocks by fluids with low X_{CO_2} and with high fluid/rock ratio infiltration (*Ferry*, 1986; *Hoish*, 1985). The contact aureoles of granitic intrusions do not often go above 700 °C (*Moore* and *Kerrick*, 1976; *Bowman* and *Essene*, 1982; *Hover-Granath* et al., 1983). Therefore, it is unlikely that wollastonite in the calcic marble was formed in a closed system at temperatures close to 700 °C. Existence of numerous faults, contacts between different lithologies, and increased porosity in carbonate rocks due to decarbonation reactions probably facilitated fluid infiltration and wollastonite formation.

The origin and nature of hydrothermal fluid

As far as the chemical composition of the hydrothermal fluid is concerned the clearest evidence comes from the fluid inclusions of those minerals that were

formed during fluid infiltration. In the case of this study the best candidate is vesuvianite. The data obtained from the fluid inclusions reveals that it is mainly an aqueous fluid, with $X_{CO_2} \sim 0.05$, a salinity around 8.7 wt.% NaCl equiv. and a density of $0.62\,g/cm^3$. The microthermometric behaviour of the volatile phase suggests a gaseous mixture consisting of $CO_2 \pm CH_4 \pm N_2$. Therefore, data obtained from the study of vesuvianite fluid inclusions suggests a metamorphic origin. Considering the C–H–O–N gaseous phase and the widespread occurrence of graphite in the laminated black shale facies of the Los Santos area (*Oczlon* and *Díez Balda*, 1992), a reaction between graphite and hydrothermal fluid ($2\,C + 2\,H_2O = CH_4 + CO_2$) may account for the formation of methane-bearing inclusions (*Roedder*, 1984). The lack of carbonaceous material in inclusions supports the hypothesis that methane was generated during fluid migration rather than during in situ reaction (*Xu*, 2000). Breakdown of organic matter or the breakdown of minerals in which K^+ is partially substituted by NH_4^+ may be considered to explain the origin of the nitrogen (*Kreulen* and *Schuiling*, 1982).

The isotopic ($\delta^{13}C$ and $\delta^{18}O$) study of silicate minerals in Los Santos skarn carried out by *Tornos* et al. (2001) also suggests a metamorphic origin. The latter authors dismiss both marine fluids and shallow meteoric waters and suggest that the fluid is of deep origin: magmatic or metamorphic. In addition, it is known that mineralized granites from the Spanish Central System (SCS) were emplaced under water-undersaturated conditions (*Locutura* and *Tornos*, 1985). As such, it would seem unlikely that igneous rocks would produce enough water to form the skarn. Therefore, the most probable origin for hydrothermal fluids is metamorphic.

Finally, the hydrothermal event recognised in Los Santos may be related to the differentiated mineralized hydrothermal events at Spanish Central System level. So, in the course of the first hydrothermal episode at about 295 ± 10 Ma, which was related with the waning Variscan orogeny the magnesian Sn–W Carro del Diablo skarn, similar to the Los Santos skarn, is developed. This skarn is located at the contact of the Rascafría-El Paular granite stock with dolomitic marbles which experienced peak temperatures of about 625 °C at a lithostatic pressure between 0.25–0.3 GPa (*Casquet* and *Tornos*, 1984). Fluids involved in this first event (Early Permian) include complex H_2O–CO_2–CH_4–NaCl fluids (*Tornos* et al., 2000).

Conclusions

Contact metamorphism was accompanied by intense metasomatism, and development of skarns, and it generated the following mineral assemblages: diopside, forsterite, phlogopite (±clintonite) and humites and spinel-bearing assemblages or diopside, grossular, vesuvianite ± wollastonite in the marbles, depending on the bulk rock composition. Cordierite, K-feldspar, andalusite and, locally, sillimanite appear in the metapelitic rocks. Mineral assemblages of marble and hornfelses indicate pressure conditions ranging from 0.2 to 0.25 GPa and maximum temperatures between 630 and 640 °C.

^{18}O- and ^{13}C-depletions in calcite marbles are consistent with externally derived hydrothermal fluid–rock interaction during metamorphism and associated metasomatism. Microthermometric analyses of fluid inclusions from vesuvianite indicate that the fluid is dominated by water with minor contents of CO_2

($\pm CH_4 \pm N_2$) suggesting a metamorphic origin. The C–H–N–O gaseous phase may have been formed by the reaction $2\,C + 2\,H_2O = CH_4 + CO_2$ between graphite from the host rocks and the hydrothermal fluids. Finally, the hydrothermal event studied in the Los Santos skarn may be correlated with the first hydrothermal episode at about $295 \pm$ Ma known from the Spanish Central System (SCS), where the magnesian Sn–W Carro del Diablo skarn, similar to the Los Santos, has developed.

Acknowledgements

This work was supported by the Comunidad Autónoma de Castilla y León (Research Project Ref. SA 073/01 and Project Ref. SA 063/03) and by an I + D Project, FEDER Program (Ref. 1FD97-0235).

References

Abart R (1995) Phase equilibrium and stable isotope constraints on the formation of metasomatic garnet-vesuvianite veins (SW Adamello, N Italy). Contrib Mineral Petrol 122: 116–133

Anovitz LM, Essene EJ (1987) Phase equilibria in the system $CaCO_3$–$MgCO_3$–$FeCO_3$. J Petrol 28: 389–414

Bakker RJ (1999) Optimal interpretation of microthermometrical data from fluid inclusions: thermodynamic modelling and computer programming. Habilitation Ruprecht-Karls-Universität, Heidelberg

Bea F, Pereira MD (1990) Estudio petrológico del Complejo Anatéctico de la Peña Negra (Batolito de Ávila). Rev Soc Geol Esp 3: 87–104

Berman RG (1988) Internally-consistent thermodynamic data for minerals in the system Na_2O–K_2O–CaO–MgO–FeO–Fe_2O_3–Al_2O_3–SiO_2–TiO_2–H_2O–CO_2. J Petrol 29: 445–522

Berman RG, Brown TH, Perkins EH (1987) GEO-CALC: Software for calculation and display of *P–T*–X phase diagrams. Am Mineral 72: 861–862

Billiton Española SA (1985) Proyecto Los Santos. Informe Final. Fase Viabilidad. Nov 83–Nov 85. Asociación PRN-BESA, 9. Informe interno. Inédito

Bottinga Y (1969) Calculated fractionation factors for carbon and hydrogen isotope exchange in the system calcite–carbon dioxide–graphite–methane–hydrogen–water vapor. Geochim Cosmochim Ac 33: 49–64

Bowman JR, Essene EJ (1982) *P–T*–X(CO_2) conditions of contact metamorphism in the Black Butte aureole, Elkhorn, Montana. Am J Sci 282: 311–340

Bowman JR, O'Neil JR, Essene EJ (1985) Contact skarn formation at Elkhorn, Montana II: Origin and evolution of C–O–H skarn fluids. Am J Sci 285: 621–660

Brown HT, Berman RG, Perkins EH (1988a) GEO-CALC: Software package for calculation and display of pressure–temperature–composition phase diagrams using an IBM or compatible personal computer. Comput Geosci 14: 279–290

Brown HT, Berman RG, Perkins EH (1988b) PTA-SYSTEM: A Geo-Calc software package for the calculation and display of activity–temperature–pressure phase diagrams. Am Mineral 74: 785–787

Bucher K, Frey M (1994) Petrogenesis of metamorphic rocks, 6th edn. Springer-Verlag, Berlin, Heidelberg, 315 pp

Casquet C, Tornos F (1984) El skarn de W–Sn del Carro del Diablo (Sistema Central Español). Bol Geol Min 95: 58–79

Chernosky JV Jr, Berman RG, Jenkins DM (1998) The stability of tremolite: New experimental data and a thermodynamic assessment. Am Mineral 83: 726–739

Craig H (1957) Isotopic standarda for carbon and oxygen and correction factors for mass-spectrometric analysis of carbon dioxide. Geochim Cosmochim Ac 12: 133–149

Crespo JL, Rodríguez P, Moro MC, Conde C, Fernández A, Rodríguez I (2000) El yacimiento de scheelita de Los Santos (Salamanca). Geotemas 1: 25–28

Deer WA, Howie RA, Zussman J (1992) An introduction to the rock forming minerals. Longman, Burnt Mill, England, 696 p

Díez Balda MA (1986) El Complejo Esquisto-Grauváquico, las series paleozoicas y la estructura hercínica al sur de Salamanca. Thesis, University of Salamanca, 279 p

Díez Balda MA, Vegas R, González Lodeiro F (1990) Structure of the Central Iberian Zone. In: *Dallmeyer RD, Martínez García E* (eds) Pre-Mesozoic Geology of Iberia. Springer, Berlin, pp 172–188

Essene EJ (1989) The current status of thermobarometry in metamorphic rocks. In: *Daly JS, Cliff RA, Yardley BWD* (eds) Evolution of Metamorphic Belts, Geological Society Special Publication 43, pp 1–44

Ferry JM (1986) Infiltration of aqueous fluid and high fluid: rock ratios during greenschist facies metamorphism: a reply. J Petrol 27: 695–714

Ferry JM (2001) Calcite inclusions in forsterite. Am Mineral 86: 773–779

Galibert F (1984) Géochimie et géochronologie du Complexe granitique de l'antiforme de Morille (Salamanque, Espagne). Rapport de Stage de DEA, Lab de Géochimie Isotopique, Univ Montpellier, 53 p

Groat LA, Hawthorne FC, Ercit TS (1992) The chemistry of vesuvianite. Can Mineral 30: 19–48

Guy B, Sheppard AM, Fouillac AM, Le Guyader R, Toulhoat P, Fonteilles M (1988) Geochemical and Isotope (H, C, O, S) Studies of Barren and Tungsten-Bearing Skarns of the French Pyrenees. In: *Boissonnas-Jean & Omenetto-Paolo* (eds) Mineral deposits within the European Community. Special publication of the Society for Geology Applied to Mineral Deposits. Springer-Verlag, New York, pp 53–75

Hendry DAF (1981) Chlorites, fengites and siderites from the Prince Lyell ore deposit, Tasmania, and the origin of the deposit. Econ Geol 76: 285–303

Hoish TD (1985) The solid solution chemistry of vesuvianite. Contrib Mineral Petrol 89: 205–214

Hover-Granath VC, Papike JJ, Labotka TC (1983) The Notch Peak Contact Metamorphic Aureole, Utah: Petrology of the Big Horse Limestone Member of the Orr Formation. Geol Soc Am Bull 94: 889–906

Julivert M, Fonboté JM, Ribeiro A, Nabais Conde LE (1972) Mapa Tectónico de la Península Ibérica y Baleares, E: 1:1.000.000. Inst Geol Min Esp

Kretz R (1983) Symbols for rock-forming minerals. Am Mineral 68: 277–279

Kreulen R, Schuiling RD (1982) N_2–CH_4–CO_2 fluids during formation of the Dôme de l'Agout, France. Geochim Cosmochim Ac 46: 193–203

Labotka TC, Nabelek PI, Papike JJ, Hover-Granath VC, Laul JC (1988) Effects of contact metamorphism on the chemistry of calcareous rocks in The Big Horse Limestone member, Notch peak, Utah. Am Mineral 73: 1095–1110

Lattanzi P, Rye DM, Rice JM (1980) Behaviour of ^{13}C and ^{18}O in carbonates during contact metamorphism at Marysville Montana: Implications for isotope systematics in impure dolomitic limestones. Am J Sci 280: 890–906

Leake BE, Woolley AR, Birch WD, Burke EAJ, Ferraris G, Grice JD, Hawthorne FC, Kisch HJ, Krivovichev VG, Schumacher JC, Stephenson NCN, Whittaker EJW (2004) Nomenclature of amphiboles: additions and revisions to the International Mineralogical Association's amphibole nomenclature. Eur J Mineral 16: 191–196

Locutura J, Tornos F (1985) Consideraciones sobre la metalogenia del sector medio del Sistema Central Español. Rev Real Acad Cienc Fis Exac Nat 59: 589–623

McCrea JM (1950) On the isotopic chemistry of carbonates and a paleotemperature scale. J Chem Phys 18: 849–857

Moore JN, Kerrick DM (1976) Equilibria in siliceous dolomite of the Alta aureole, Utah. Am J Sci 276: 502–524

Olesch M (1975) Synthesis and solid solubility of trioctahedral brittle micas in the system $CaO–MgO–Al_2O_3–SiO_2–H_2O$. Am Mineral 60: 188–199

Olesch M, Seifert F (1976) Stability and phase relations of trioctahedral calcium brittle micas (Clintonite Group). J Petrol 17: 291–314

Ozclon MS, Díez Balda MA (1992) Contourites in laminated black shale facies of the Aldeatejada Formation (Precambrian/Cambrian boundary range, province of Salamanca, Western Spain). Rev Soc Geol España 5: 167–176

Piazolo S, Markl G (1999) Humite- and Scapolite-bearing assemblages in marbles and calc-silicates of Droning Maud Land, East Antarctica: new data for Gondwana reconstructions. J Metamorph Geol 17: 91–107

Pinarelli L, Rottura A (1995) Sr and Nd isotopic study and Rb–Sr geochronology of the Bejar granites, Iberian Massif, Spain. Eur J Mineral 7: 577–589

Powell R, Holland T (1990) Calculated mineral equilibria in the pelite system, KFMASH ($K_2O–FeO–MgO–Al_2O_3–SiO_2–H_2O$). Am Mineral 75: 367–380

Rice JM (1977) Progressive metamorphism of impure dolomitic limestone in the Marysville Aureole, Montana. Am J Sci 277: 1–24

Rice JM (1979) Petrology of clintonite-bearing marbles in the Boulder aureole, Montana. Am Mineral 64: 519–526

Rice JM (1980a) Phase equilibria involving humite minerals in impure dolomitic limestones, Part I. Calculated stability of clinohumite. Contrib Mineral Petr 71: 219–235

Rice JM (1980b) Phase equilibria involving humite minerals in impure dolomitic limestones. Part II. Calculated stability of chondrodite and norbergite. Contrib Mineral Petr 75: 205–223

Robinson P, Spear FS, Schumacher JC, Laird J, Klein C, Evans BW, Doolan BL (1982) Phase relations of metamorphic amphiboles: natural occurrence and theory. In: *Veblen DR, Ribbe PH* (eds) Amphiboles: Petrology and experimental phase relations. Rev Mineral Mineral Soc Am 9B: 69–760

Roedder E (1984) Fluid inclusions. Mineral Soc Am Rev Mineral 12: 12–45

Rottura A, Bargossi GM, Carioni V, D'Amico C, Maccarrone E (1989) Petrology and geochemistry of late-Hercynian granites from the Western Central System of the Iberian Massif. Eur J Mineral 1: 667–683

Saavedra J, García Sánchez A (1973) Composición química de las biotitas de granitos de la provincia de Salamanca relacionada con las condiciones de formación. Stud Geol VI: 7–27

Satish-Kumar M, Wada H, Santosh M, Yoshida M (2001) Fluid-rock history of granulite facies humite-marbles from Ambasamudram, southern India. J Metamorph Geol 19: 395–410

Sheperd TJ, Rankin AH, Alderton DHM (1985) A practical guide to fluid inclusions studies (Blackie Ed) Glasgow

Shieh YN, Taylor HP (1969) O and C isotope studies of contact metamorphism of carbonate rocks. J Petrol 10: 307–331

Spear FS (1993) Metamorphic phase equilibria and pressure–temperature–time paths: Mineralogical Society of America Monograph, 799 pp

Taylor HP (1974) An application of oxygen and hydrogen isotope studies to problems of hydrothermal alteration and ore deposition. Econ Geol 69: 843–883

Taylor HP (1977) Water/rock interactions and origin of H_2O in granitic batholits. Geol Soc London J 133: 509–559

Tornos F, Delgado A, Casquet C, Galindo C (2000) 300 Million years of episodic hydrothermal activity: stable isotope evidence from hydrothermal rocks of the Eastern Iberian Central System. Miner Deposita 35: 551–569

Tornos F, Galindo C, Spiro BF (2001) Isotope geochemistry of Los Santos (Spanish Central System) calcic scheelite skarn: constraints on the source of the fluids and tungsten. In: *Piestrzynski* et al. (eds) Mineral Deposits at the Beginning of the 21st Century. Swets & Zeitlinger Publishers Lisse, 921–924

Ugidos JM (1987) Características del metamorfismo de baja presión en zonas centro-occidentales españolas y su significado en relación con minerales alumínicos en los granitos. Mem Mus Labor Miner Geol Fac Ciências do Porto 1: 383–398

Ugidos JM, Recio C (1993) Origin of cordierite-bearing granites by assimilation in the Central Iberian Massif (CIM), Spain. Chem Geol 103: 27–43

Valley JW (1986) Stable isotope geochemistry of metamorphic rocks. In: *Valley JW, Taylor HP Jr, O'Neil JR* (eds) Stable isotopes in high temperature geological processes. Washington DC. Mineral Soc Am Rev Mineral 16: 445–489

Valley JW, Petersen EU, Essene EJ, Bowman JR (1982) Fluorphlogopite and fluortremolite in Adirondack marbles and calculated C–O–H–F fluid compositions. Am Mineral 67: 545–557

Valley JW, Peacor DR, Bowman JR, Essene EJ, Allard MJ (1985) Crystal chemistry of a Mg-vesuvianite and implications for phase equilibria in the system $CaO–MgO–Al_2O_3–SiO_2–H_2O–CO_2$. J Metamorph Geol 3: 137–153

Van den Kerkhof AM, Thiéry R (2001) Carbonic inclusions. Lithos 55: 49–68

Veizer J, Hoefs J (1976) The nature of $^{18}O/^{16}O$ and $^{13}C/^{12}C$ secular trends in sedimentary carbonate rocks. Geochim Cosmochim Ac 40: 1387–1395

Wiewióra A, Weiss Z (1990) Crystallochemical classifications of phyllosilicates based on the unified systems of projection of chemical compositions: II. The chlorite group. Clay Miner 25: 83–92

Xu G (2000) Methane-rich fluid inclusions in the Proterozoic Zn–Pb–Ag deposit at Dugald River, NW Queensland: potential as an exploration guide. Applied Geochemistry 15: 1–12

Yenes M, Gutiérrez-Alonso G, Álvarez F (1996) Dataciones K–Ar de los granitoides del área La Alberca-Bejar (Sistema Central Español). Geogaceta 20: 224–227

Yenes M, Álvarez F, Gutiérrez-Alonso G (1999) Granite emplacement in orogenic compressional conditions: the La Alberca-Bejar granitic area (Spanish Central System, Variscan Iberian Belt). J Structural Geol 21: 1419–1440

Zheng YF (1999) Oxygen isotope fractionation in carbonate and sulfate minerals. Geochem J 33: 109–126

Authors' addresses: *S. M. Timón* (corresponding author; e-mail: stimon@usal.es), *M. C. Moro*, *M. L. Cembranos* and *A. Fernández*, Departamento de Cristalografía y Mineralogía, Facultad de Ciencias, Universidad de Salamanca, Plaza de la Merced, s/n 37008 Salamanca, España, *J. L. Crespo*, SIEMCALSA, Incas 5, 47008 Valladolid, España